

DUAL-USE STRAIN SENSORS FOR ACOUSTIC EMISSION AND QUASI-STATIC BENDING MEASUREMENTS

JASON MATTHEW STIEFVATER

Thesis submitted to the faculty of the Virginia Polytechnic Institute and State University in partial fulfillment of the requirements for the degree of

Master of Science
In
Mechanical Engineering

Wing F. Ng, Chair
Alfred L. Wicks
Robert L. West

May 4, 2023
Blacksburg, VA

Keywords: Acoustic Emission, NDE, SHM, MEMS, Strain Sensor, Source Location, Plate Bending

DUAL-USE STRAIN SENSORS FOR ACOUSTIC EMISSION AND QUASI-STATIC BENDING MEASUREMENTS

JASON MATTHEW STIEFVATER

ABSTRACT

The application of piezoelectric sensors such as the ultrasonic transducer has significantly enhanced the fields of nondestructive evaluation (NDE). Their application of piezoelectric materials allows for the sensing of low energy, high frequency acoustic emission (AE) events such as fatigue cracking in metals and delamination in composites. Utilizing the physical characteristics of these AE waves, the location of these structural defects can then be source located by means of time-of-flight trilateration. The real time sensing of such events has led to the field of structural health monitoring (SHM) and has revolutionized NDE. Furthermore, with the application of modern micro-electromechanical system-based (MEMS) technology, the fields of NDE and SHM can be improved greatly, and sensing instrumentation simplified.

A novel piezoresistive-based MEMS strain sensor is presented as this improvement to NDE and SHM. The ultrathin silicon membrane-based (USM) strain sensor's ability to capture an AE signal is demonstrated by a Hsu-Nielsen source and shows comparable frequency content to a commercial piezoceramic ultrasonic transducer. To the knowledge of the authors, this makes the USM strain sensor the first known piezoresistive strain sensor capable of recording low energy AE. The novel improvements to NDE and SHM arise from the sensor's low minimum detectable strain and wide frequency bandwidth, enabling a dual-use application of both AE and static strain sensing. The USM sensor's ability to document quasi-static bending is demonstrated and once again compared with an ultrasonic transducer, which provides no significant response. This dual-use application is proposed to effectively combine the uses of both strain and ultrasonic transducer sensor types within one sensor, lending itself novel and useful to NDE and SHM. The potential benefits include enhanced sensitivity, reduced sensor size and cost, and reduced instrumentation complexity.

DUAL-USE STRAIN SENSORS FOR ACOUSTIC EMISSION AND QUASI-STATIC BENDING MEASUREMENTS

JASON MATTHEW STIEFVATER

GENERAL AUDIENCE ABSTRACT

Visual inspection for cracks and defects has long been staples of assessing structural health throughout human history. These surface imperfections are an obvious hindrance to structural integrity and routine observation and inspection is needed to ensure a structure's safety. With the progression of technology and the discovery of piezoelectric materials, more advanced methods have been devised to detect and source locate not only surface level but sub-surface cracking. This has been accomplished through the use of piezoelectric ultrasonic transducers to monitor the propagation of acoustic emission (AE) vibrations, which are the result of energy redistribution by events such as cracking. The remote monitoring of AE events has led to the growth of the nondestructive evaluation (NDE) field, where these cracks and defects can be located by the detection of their AE source. These transducers, however, are met with limitations in their applications. Operating off the piezoelectric effect allows for a superb response to low energy, high frequency excitation characteristic of AE, but results in no response to quasi-static strain measurements, such as that of a slowly applied bending load on a plate.

In the work herein, modern micro-electromechanical system (MEMS) based technology is utilized to devise a sensor capable of both AE and static strain measurements. The dual sensing of both of these measurements can allow for the source location of cracking events along with the monitoring of structure strain, effectively combining the use of two sensors into one. This dual-application use can have a great impact on the evaluation of critical structures like bridges and aircraft and simplify and reduce costs inherent to nondestructive evaluation.

PREFACE

The work presented in this thesis covers the various applications of a novel piezoresistive strain sensor to the fields of nondestructive evaluation and structural health monitoring. The sensor's ability to detect low energy acoustic emission is demonstrated and analyzed in addition to bending strain sensing, which is typically characteristic of a piezoresistive strain sensor. The importance of these sensing abilities is presented as its potential dual-application sensing to critical structures such as bridges and aircraft.

The National Aeronautics and Space Administration (NASA) provided funding for this research project. NanoSonic Inc. sponsored this research project and provided the USM strain sensor, signal conditioning board and box, and additional necessary testing apparatus and laboratory equipment. The author was involved in all aspects of the research work, including the experimental setup design and build, data acquisition, data reduction, and data analysis. Throughout his M.S. program, the author worked closely with two NanoSonic employees Albrey de Clerck and Noah Jones.

The primary objectives of this research work are as follows:

- I. Demonstrate the USM strain sensor's ability for dual application sensing.
- II. Apply acoustic emission source location techniques using the USM strain sensor.
- III. Explore and apply the USM strain sensor to other areas of nondestructive evaluation.

This thesis mainly consists of a journal article with additional research relevant to the main body article and primary research objectives presented in the appendices. The journal article presents the USM strain sensor as the first piezoresistive strain sensor capable of low energy acoustic emission detection and its novel dual application sensing. This article is being prepared for submission in the journal of Structural Health Monitoring. The appendices include additional supplementary materials and methods relevant to the article, as well as additional research that plans to be rewritten and submitted to another journal at a later date. This work includes preliminary results in acoustic emission source location by the USM strain sensor of both a Hsu-Nielsen source and a high velocity impact and exploring other aspects of NDE including demonstrating the sensor's ability to differentiate the energy of impacts and sensor response to a vibrating plate in the form of a Chladni figure.

ACKNOWLEDGEMENTS

First, I would like to thank my entire family, particularly my mother Mary Lou Stiefvater, father Todd Stiefvater, brother Robert Stiefvater, and Aunt Tracy Stiefvater. I am forever grateful for their unwavering love, support, and sacrifices, which without none of this would have been possible.

Next, I would like to thank and acknowledge my advisor Dr. Ng for the opportunity to participate in his research which has allowed me to further my education. I would also like to thank Dr. Ng and committee members Dr. Wicks and Dr. West for their many insights and guidance throughout this research.

Lastly, I would like to thank and acknowledge members of the NanoSonic Inc. team Dr. Hang Ruan, Dr. Echo Kang, Albrey de Clerck, and Noah Jones. Their collective knowledge of the engineering sciences and continuous support has incredibly enhanced the present work and has undoubtedly made me a better engineer and scientist. It has been a pleasure and an honor to work with them.

Table of Contents

List of Figures	vii
NOMENCLATURE	1
1. INTRODUCTION	1
2. MATERIALS AND METHODS.....	3
2.1 Governing Physics	3
2.1.1 Acoustic Emission in Isotropic Thin Aluminum Plates.....	3
2.1.2. Quasi-Static Plate Bending	3
2.2 Experimental Setup.....	3
2.2.1 Acoustic Emission Testing	3
2.2.2 Quasi-Static Plate Bending Testing	4
3. RESULTS AND DISCUSSION	4
3.1 Sensor Response to Acoustic Emission	4
3.1.1 Time Domain Analysis	4
3.1.2 Frequency Domain Analysis.....	5
3.2 Sensor Response to Quasi-Static Bending.....	6
4. CONCLUSIONS AND FUTURE WORK	8
ACKNOWLEDGEMENTS.....	9
REFERENCES	9
ATTRIBUTIONS	11
APPENDIX A: SUPPLEMENTARY MATERIALS.....	12
APPENDIX B: AE SOURCE LOCATION PRELIMINARY RESULTS	17
APPENDIX C: OTHER NDE APPLICATIONS OF THE USM STRAIN SENSOR.....	19

List of Figures

Figure 1. Microscopic images of the fabricated silicon membrane-based strain sensors.	2
Figure 2. Schematic of the aluminum 6061-T6 testing plate.	2
Figure 3. Schematic representation of the acoustic emission testing experimental setup.	4
Figure 4. Schematic representation of the quasi-static bending testing experimental setup.	4
Figure 5. Time domain analysis of the USM strain sensor response to acoustic emission.	5
Figure 6. PSD of the filtered AE data from both sensor types.	6
Figure 7. Bending strain loading performance of the USM strain sensor.	8
Figure A1. Experimental setup of the acoustic emission testing.	12
Figure A2. Unfiltered acoustic emission sensor signals.	12
Figure A3. Analog to digital converter (ADC) noise in PicoScope 5444D.	13
Figure A4. PSD of the unfiltered noise signal in the USM strain sensor.	14
Figure A5. Custom-made static plate holder for quasi-static loading.	14
Figure A6. NanoSonic Inc. signal conditioning box used in quasi-static bending strain testing.	15
Figure A7. Instron loading curves for quasi-static loading experiments.	15
Figure A8. Unfiltered responses to quasi-static bending strain across various constant loading rates.	16
Figure B1. The “bilateration” of an AE source (PLB) using the extensional mode.	17
Figure B2. The “bilateration” of a high velocity impact using the flexural mode.	18
Figure C1. Experimental setup for vibrating plate testing.	19
Figure C2. Schematic of the vibrating plate COMSOL Multiphysics model boundary conditions.	19
Figure C3. Drop testing experimental setup.	20
Figure C4. Impact study plate setup.	20
Figure C5. Six example mode shapes across a frequency range of 5 Hz – 7.5 kHz compared to the model.	20
Figure C6. Comparing the frequency domain response across five plate modal frequencies.	21
Figure C7. Recorded drop test data for the two USM and one metal-based strain sensor for location 1.	21
Figure C8. USM strain sensor voltage RMS plotted as a function of the initial drop potential energy.	21
Figure C9. Observed latency between USM strain sensors at drop location 1.	22
Figure C10. Observed latency between USM strain sensors as a function of seven drop locations.	22

DUAL-USE STRAIN SENSORS FOR ACOUSTIC EMISSION AND QUASI-STATIC BENDING MEASUREMENTS

Jason Stiefvater¹, Yuhong Kang², Albrey de Clerck², Shuo Mao¹, Noah Jones², Josh Deem²,
Hang Ruan^{1,2*}, Wing Ng^{1*}

¹Department of Mechanical Engineering, Virginia Tech; Blacksburg, VA 24061

²NanoSonic, Inc.; 158 Wheatland Drive, Pembroke, VA 24136

NOMENCLATURE

a_o	Axisymmetric mode
S_o	Symmetric mode
σ	Stress
E	Elastic modulus
P	Concentrated point load
t	Plate thickness
b	Plate length
ν	Poisson's ratio
e	Radius of applied load

1. INTRODUCTION

Nondestructive evaluation (NDE) is crucial in assessing structural integrity by detecting imperfections and damages such as fatigue cracking, high velocity impacts, and delamination through the sensing of acoustic emission (AE) (1). The nondestructive nature of the testing lends itself well to the assessment of permanent structures such as bridges, for repetitive use items subject to fatigue cracking such as airplane wings, and even monitoring projectile impacts on spacecraft. Its applications in these fields make NDE imperative to their safety and performance. Originally by purely visual inspection, techniques for flaw detection have been employed throughout history to assess the quality of structures. While visual inspection remains, complex instrumentation is now supplementarily utilized in NDE to assess subsurface structural damage unobservable to the eye and to reduce the need of routine inspection. The introduction of such complex instrumentation has undoubtedly furthered the field of NDE and improved the safety of many crucial aforementioned industries. However, with continuous advancements in manufacturing and technology, advances in nondestructive testing and evaluation (NDT&E) must keep pace. This calls for improvement in testing instrumentation and data collection with the goal of realizing a seamless connection with the requirements of modern technology (2).

The sensing of vibrations within NDE typically exists in two categories: active and passive measurements. The scope of this work focuses on measurement and analysis by the application of passive sensing, where sensors measure excitation created by a controlled outside source (3, 4). A common tool for passive and active measurement within NDE is the piezoelectric ultrasonic transducer, which exists in a broad range of frequency bandwidths, typically operating in

resonance between 200 kHz – 10 MHz (5). The sensor's high sensitivity and high frequency response enables their use in capturing acoustic emission. These low energy, high frequency stress waves are emitted by the propagation of surface level and sub-surface cracks and imperfections within a structure caused by the redistribution of strain energy (6-8). Additional post-processing of these signals can reveal the approximate location of the AE source, which is especially useful for locating sub-surface level cracking not caught by visual inspection. Many studies have been performed on the source location of AE events, and it has been the focus of many studies to improve the fields of nondestructive evaluation and structural health monitoring (SHM) (7-13).

Piezoelectric sensors convert dynamic forces into electrical signals by means of the piezoelectric effect and can accurately measure rapid strain changes without latency (14). However, this generated voltage quickly dissipates to the surroundings due to its easily neutralized surface charge (14, 15). This prevents the utilization of piezoelectric sensors in the sensing of bending strain, which is an important measurement in both aerospace and civil structures alike (16, 17). The use of piezoelectric ceramic materials such as lead zirconate titanate (PZT) within transducers has enabled wider frequency bandwidths, allowing their use in broader applications (18-21). Linsheng Huo et al. (2017) reported the use of a PZT transducer to closely match the signal of a strain sensor in a dynamic bending failure test of reinforced concrete, demonstrating PZT transducers' potential for documenting lower frequency vibrations and, in a sense, measuring strain by a comparison between signals with a piezoresistive strain sensor (3). However, the dynamic bending test was performed with a quickly applied load (60 mm/s) and proceeds past the concrete's elastic limit until fracture, which does not evaluate the PZT transducer's performance to static bending strain measurement.

In this study, the authors report the first experimental measurement of low energy acoustic emission with a piezoresistive MEMS strain sensor; additionally, the sensor's ability for dual application of both quasi-static bending strain and high frequency acoustic emission sensing is demonstrated. Shown in Figures 1 and 2, the piezoresistive ultrathin silicon membrane (USM) based strain sensor is fabricated on a silicon on insulator (SOI) wafer and transferred to a polyimide based flexible substrate with electrical interconnections. The membrane thickness varies from a few hundred nanometers to

a few microns with minimum lateral dimensions at least two orders of magnitude greater than the thickness. The SOI based silicon membranes are gaining acceptance in the semiconductor industry, as the benefits they provide become key enablers in scaling and performance enhancements of electric devices since the initial fabrication was introduced by John Rogers' group (22). At this time, the improved sensor fabrication process to permit crystalline membrane and advanced polymers to be co-processed in a way that controls the sensitivity and dynamic range of the sensor elements is proprietary to NanoSonic Inc.

Typical metal and semiconductor piezoresistive strain sensors are historically reserved for static bending and low frequency applications due to their large sensing element size and sensitivity restricting their frequency bandwidth and minimum detectable strain (23). For this reason, these commercial strain sensors function well in measuring quasi-static and low frequency bending strain, but fail to record low energy, high frequency AE. The presented miniaturized ultrathin silicon membrane-based strain sensor fabricated by NanoSonic Inc. serves to bridge this gap in frequency bandwidth between ultrasonic transducers and strain sensors by utilizing a piezoresistive micron-scale sensing element which enables a wide frequency bandwidth response and a low minimum detectable strain. The objective of the work herein is to demonstrate NanoSonic's strain sensor's ability to reliably document low energy, high frequency AE signals, making it,

to the knowledge of the authors, the first known piezoresistive strain sensor technology capable of recording low energy AE, as well as reliably document bending strain. By the dual monitoring of both bending strain measurements and AE events, the uses of multiple sensors can effectively be condensed into one strain sensor, reducing costs, sensor size, and instrumentation complexities associated with NDE and SHM.

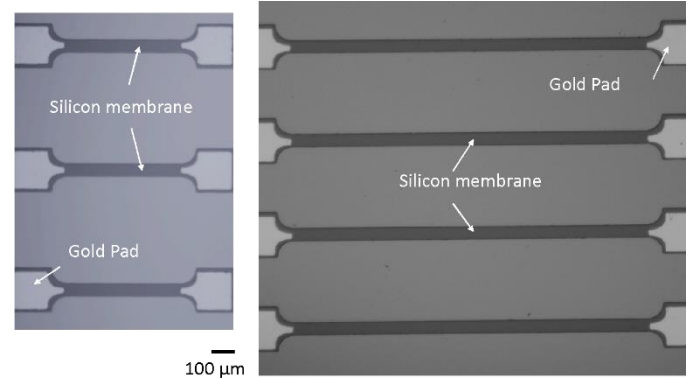


Figure 1. Microscopic images of the fabricated silicon membrane-based strain sensors of different sizes on SOI wafers, transferred to polyimide substrates for AE and strain measurements. The membrane thickness varies from a few hundred nanometers to a few microns.

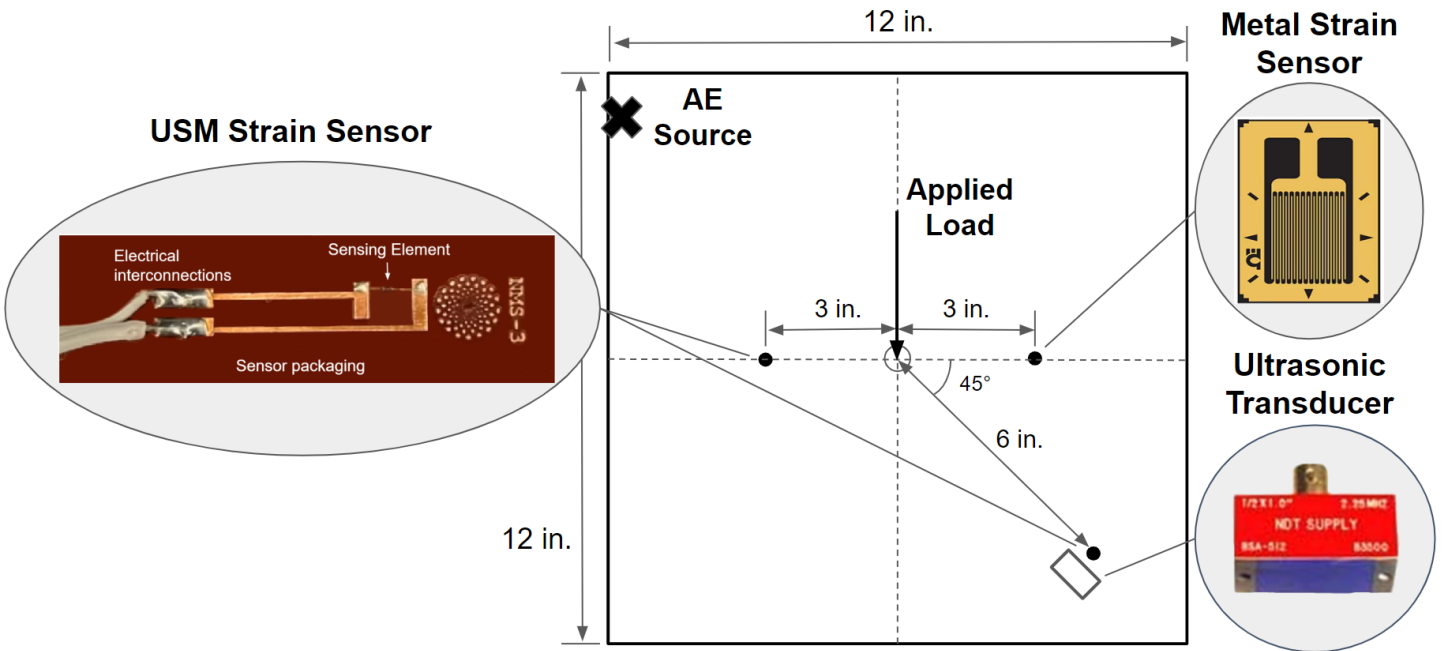


Figure 2. Schematic of the aluminum 6061-T6 testing plate with mounted piezoresistive ultrathin silicon membrane (USM) based strain sensor and commercial sensors. Two USM strain sensors (sensing element: length/width/thickness: 500 µm/60 µm/4 µm) are mounted on the aluminum plate (2.2 mm thickness) with a Britek 2.25 MHz PZT ultrasonic transducer and a commercial Omega metal-based linear strain sensor (sensing element length: 11.8 mm). The bottom right USM strain sensor is utilized in acoustic emission experimentation and the leftmost sensor in quasi-static bending experimentation.

2. MATERIALS AND METHODS

This section begins with a brief discussion of the necessary background information of the physics behind acoustic emission in isotropic thin aluminum plates and quasi-static bending. Next, the experimental setup and necessary information on experiment replicability for the acoustic emission and bending tests are discussed. Supplementary materials can be found in Appendix A.

2.1 Governing Physics

2.1.1 Acoustic Emission in Isotropic Thin Aluminum Plates

Within plate-like elements (where thickness is considerably less than the other two plate dimensions), Lamb waves are the dominant mode of AE propagation (24). These waves occur as two basic modes: symmetric (S_0) and asymmetric (a_0) (also referred to as extensional and flexural modes, respectively) (13). Higher order modes can exist but are typically low energy, particularly in thin plates (where AE wavelengths are much larger than plate thickness) and are insignificant in AE applications (8). An important attribute of the extensional (S_0) wave is that it acts as a precursor to the flexural wave and is essentially non-dispersive; however, it is typically much lower amplitude and higher frequency. The non-dispersive nature of the extensional wave makes it much easier for time-of-flight AE source location techniques to be applied, but its low amplitude, high frequency content makes it difficult to sense. The flexural (a_0) wave, on the other hand, typically has a much greater amplitude and is highly dispersive, meaning its frequency content separates with time as its higher frequencies propagate faster. Due to the inherent tradeoffs between source location techniques of the extensional and flexural modes, an accurate recording of both AE modes is desired. These acoustic emission waves within thin plates have been extensively studied and characterized and their respective frequency content documented using PZT ultrasonic transducers (24, 25). For these reasons, a thin aluminum plate was utilized to study the USM strain sensor's performance in sensing AE.

The pencil lead break, commonly referred to as a Hsu-Nielson source based on the popularization of the method by Hsu and Nielsen (26), is a long-established standard as a reproducible artificial AE source within thin plates. The PLB resembles real crack formation/AE phenomenon and produces both extensional and flexural AE modes within thin plates (11). This technique is used in the present experimentation to repeatably generate AE within a thin aluminum plate.

2.1.2. Quasi-Static Plate Bending

In this experiment, a slowly increasing load is applied to the center of the plate to apply quasi-static bending. Within solid mechanics, the quasi-static bending of a plate implies the loading occurs at a slow enough rate where inertial effects and

forces are negligible. At the macroscopic level, the stress versus strain curve under quasi-static loading now monotonically increases (27), meaning the relationship only increases with respect to one another. Assuming a 1D stress state, small plate deflections and loading occurring only in the elastic region, the loading is entirely time-independent and the stress versus strain curve increases linearly. The bending stress for a simply supported rectangular flat plate (zero edge deflection and bending moment) with a concentrated center load follows Equation 1:

$$\sigma = \frac{1.5P}{\pi t^2} \left((1 + \nu) \ln \left(\frac{2b}{\pi e} \right) + k_2 \right) \quad (1)$$

where $k_2 = 0.435$ for a square plate. Since e is sufficiently large (greater than half of the plate thickness), a correction factor for the applied load radius is not needed (28, 29). The primary takeaway is the bending stress in this loading case linearly increases with the applied load; therefore, so does the elastic strain. As the applied load on the center of the plate increases, the strain sensors should output a linear response (increasing if in tension, decreasing if in compression).

2.2 Experimental Setup

2.2.1 Acoustic Emission Testing

The position of the acoustic emission source (PLB) relative to the sensors is shown in Figure 3. This position was chosen as it was the farthest away from the previously mounted USM sensor; the location was offset an inch lower in the Y axis to avoid interference from the center plate hole. USM sensor "A" was also chosen for AE experimentation as its location allows for a farther AE source, which allows for greater separation of the extensional and flexural AE modes (25). The PZT ultrasonic transducer was placed next to the USM strain sensor "A" in such a way that both sensing elements would be subjected to the traveling acoustic emission stress waves at approximately the same time, from a source approximately 14 inches away.

The thin aluminum plate with mounted sensors laid flat on a foam backed support layer. The strain sensors (USM and metal-based) signals went directly to the signal conditioning board, which was supplied with ± 5.7 V of power by an external power supply. The board is based on a Wheatstone bridge configuration to convert change in strain sensor resistance to an amplified output voltage. Strain sensor leads are taken as input (USM or metal-based) and the board utilizes a potentiometer to balance the bridge. An INA118 instrumentation amplifier is used with a ~ 1 k Ω gain resistor to set the amplification gain to approximately 51 for the output signal. The output of the signal conditioning board is sent to the PicoScope 5444D for data acquisition. The ultrasonic transducer output went directly to the PicoScope. This experimental setup can be seen in Figure A1. Data was collected for 50 ms at 17.86 MHz to ensure the entire AE signal and subsequent reflections were captured and any

aliasing effects avoided. A rising slope trigger was placed on the transducer signal to begin data acquisition.

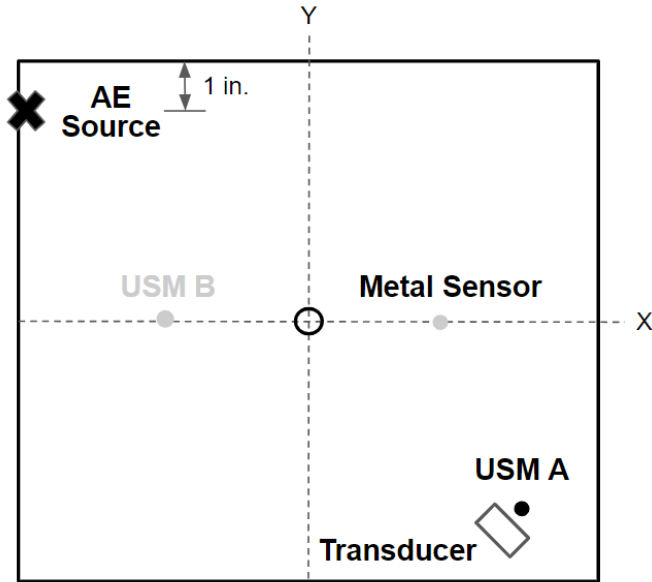


Figure 3. Schematic representation of the acoustic emission testing experimental setup. Testing was performed on an aluminum 6061-T6 12-inch square plate with 0.087-inch thickness.

2.2.2 Quasi-Static Plate Bending Testing

Presented in Figure 4, the center of the plate was loaded with a simulated point load utilizing a metal pin and the Instron 3369 machine. The plate rests on a custom-made static plate holder to provide a simply supported plate boundary condition. A greater explanation of this custom plate holder can be seen in Figure A5. Since USM sensor “B” is closer to the center loading of the plate, it is subjected to a greater bending stress and therefore outputs a greater response to the loading. For this reason, USM sensor “B” was utilized for this test. To ensure both the USM strain sensor and the ultrasonic transducer are subject to the same loading, the plate was flipped upside-down, and the transducer was placed directly over top of the USM sensor. The difference in tension versus compression is accounted for in post-processing by multiplying the transducer data by negative one.

The strain sensor signals (USM and metal) are routed to a NanoSonic Inc. signal conditioning box. The box uses a similar Wheatstone bridge configuration with potentiometers to output strain sensor signals (Fig. A6). It houses its own internal power supply, and because of this the output voltage is met with additional noise. The NanoSonic team is working on another signal conditioning box with an internal power supply with reduced noise and an improved signal to noise ratio. Output signals from this box are sent to a PicoScope 5444D for data acquisition. Data was sampled at 200 kHz for 5 seconds for the 1 mm/s and 2 mm/s tests, 500 kHz for 2

seconds for the 4 mm/s test, and 1 MHz for 1 second for the 8 mm/s test. A rising slope trigger was placed on the USM sensor signal to begin data acquisition.

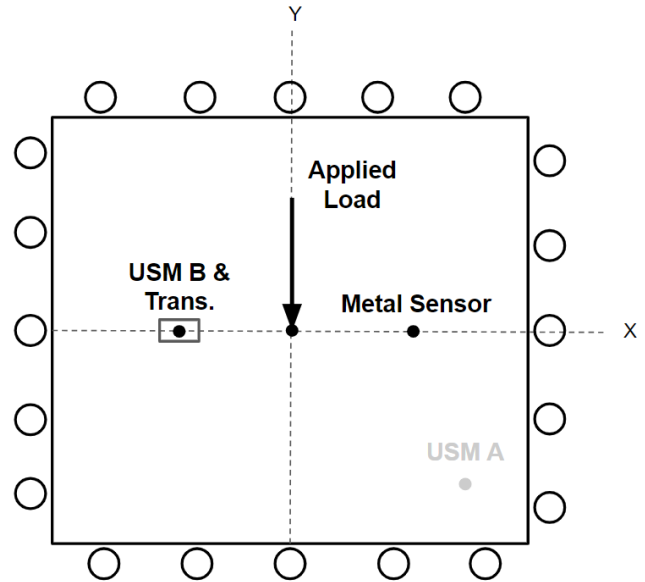


Figure 4. Schematic representation of the bending strain testing experimental setup. Testing was performed on an aluminum 6061-T6 12-inch square plate with 0.087-inch thickness.

3. RESULTS AND DISCUSSION

Once experimental data was collected, MATLAB was utilized for all data processing. MATLAB’s Signal Processing Toolbox was used for cross-correlation and power spectral density calculations. Analysis of the respective sensor responses to acoustic emission was split into signal similarities in the time and frequency domains. The results of respective sensor performances to acoustic emission and quasi-static bending are described in this section.

3.1 Sensor Response to Acoustic Emission

3.1.1 Time Domain Analysis

Notably, the USM strain sensor captures the AE generated by the Hsu-Nielson source, as well as the ultrasonic transducer. Figure 5 shows the filtered recorded signal of both sensors. The USM strain sensor documents both the flexural (a_o) and extensional mode (S_o) from the AE source. The small amplitude, high frequency extensional mode is seen immediately following the zeroed time of strain arrival, which is succeeded by the larger amplitude flexural mode. The USM strain sensor’s apparent ability to record the extensional wave makes it a strong candidate to replace ultrasonic transducers in AE sensing, as it can be used for extensional wave-based time-of-flight AE source location. A more complex method of AE source location in thin plates, demonstrated by Gorman and Ziola (9), utilizes the dispersive flexural wave and cross-

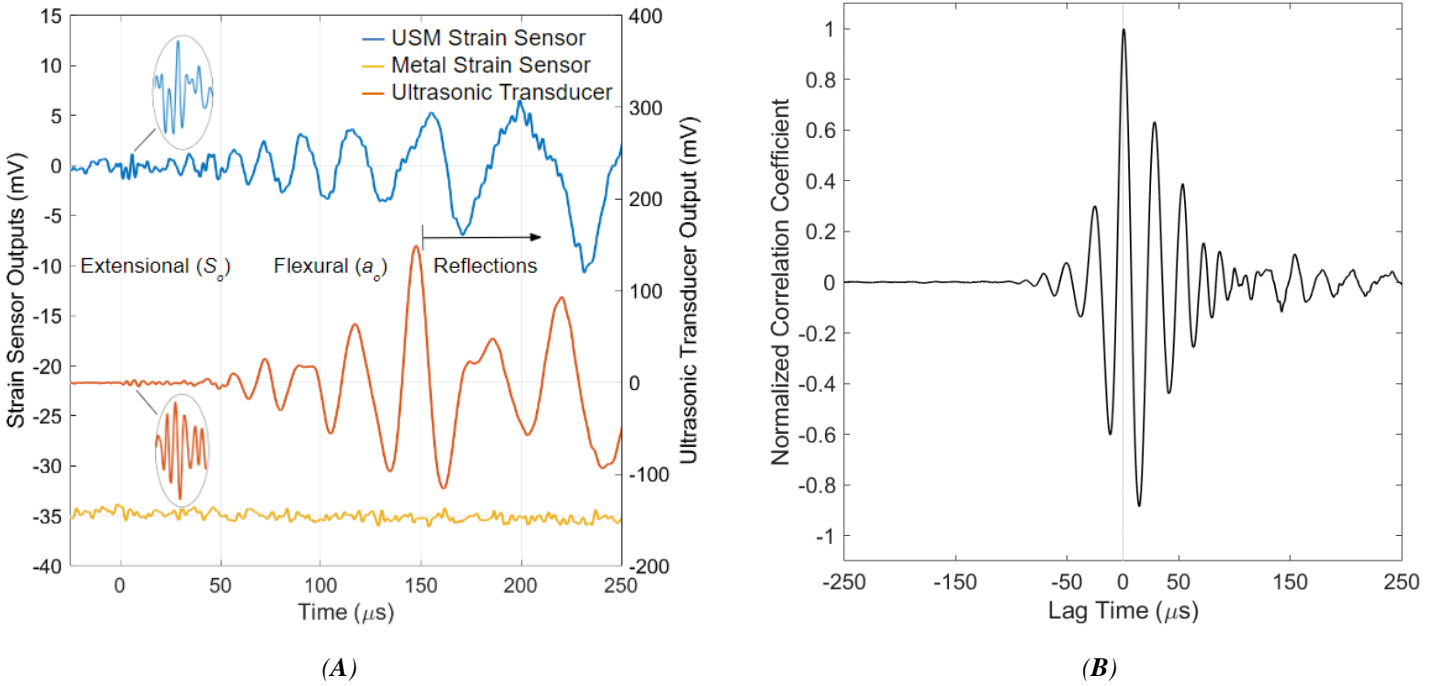


Figure 5. Time domain analysis of the USM strain sensor response to acoustic emission compared to an ultrasonic transducer generated by a Hsu-Nielsen source. (A) The recorded AE signals plotted as a function of time. The USM strain sensor signal (blue trace) and the commercial metal-based strain sensor (yellow trace) are plotted on the same left y-axis scale; the commercial 2.25 MHz broadband ultrasonic transducer (orange trace), is plotted on the right y-axis scale. Measured AE signal characteristics (extensional and flexural modes) are labeled along with subsequent plate-end reflections beginning at approximately 150 μs after first strain arrival. The signals were digitally filtered with a gaussian-weighted moving average filter. **(B)** Normalized cross-correlation between the filtered AE signals of the USM strain sensor and the ultrasonic transducer for the 100 μs preceding and 150 μs following first strain arrival.

correlation, further validating the USM strain sensor's potential in AE source location.

Between the times of strain arrival and approximately 150 μs, the ultrasonic transducer and USM strain sensor capture nearly identical signals, barring noise in the USM strain sensor signal. This noise is presumably a result of electromagnetic interference (EMI) from the surrounding laboratory instrumentation and the sensor signal conditioning board. The NanoSonic Inc. team is already working to develop a more EMI resistant sensor packaging and signal conditioning unit to improve the sensor's signal to noise ratio. The cross-correlation between filtered USM strain sensor and ultrasonic transducer AE signals in Figure 6 further illustrates the strong similarity in documented signals. A maximum correlation is observed at approximately zero lag time, demonstrating that the strongest correlation between sensor signals occurs at the zeroed time of strain arrival. This verifies the time resolution and sensitivity of the USM strain sensor as it begins signal excitation at the same time of strain arrival as the ultrasonic transducer, as both sensors were equidistant from the AE source. Following 150 μs, plate-end reflections begin influencing the recorded signals. Previously seen in Fig. 2, the ultrasonic transducer is placed directly next to the USM strain sensor, which is mounted on the plate's diagonal. Since the two sensors are in slightly different positions relative to the

plate edges, they are subject to different plate-end reflections and therefore capture different signals after 150 μs. The commercial metal-based strain sensor is unable to provide any significant response to the AE excitation due to a limited frequency bandwidth as a result of its large sensing element size.

3.1.2 Frequency Domain Analysis

Additional analyses were performed to compare frequency content of the USM strain sensor and ultrasonic transducer's respective AE signals and to verify their similarity; the metal strain sensor is omitted from frequency analysis due to its non-responsiveness to AE. Figure 6 begins this comparison by plotting the power spectral density (PSD) of the filtered sensor signals. The transducer results are consistent with AE spectral results done by Gorman (1991), with the spectral plot consisting of two distinct regions: a higher energy, lower frequency flexural mode, and a lower energy, higher frequency extensional mode of vibration present within the AE signal (25). These results are expected from the transducer as it has been previously shown to be a reliable tool in capturing flexural and extensional modes of vibration, thus making them a qualified benchmark for comparison in AE sensing. Notably, the USM strain sensor shows very similar frequency windows as the transducer. The USM sensor

records a flexural mode window spanning approximately 17.4 – 122 kHz compared to the transducer’s 17.4 – 131 kHz. The nearly identical flexural mode frequency content further validates the accuracy of the flexural mode AE signal captured by the USM strain sensor.

The two sensors also capture comparable extensional mode frequency content. The transducer captures a distinct extensional mode peak at 249 kHz, whereas the USM sensor records one at 214 kHz. Similar but not identical, one potential cause for this discrepancy in extensional mode peak frequency is distortion in the USM strain sensor signal due to the previously mentioned high frequency EMI and noise in the sensor’s signal conditioning unit. The noise can be seen in Fig. 3B directly following the extensional mode peak from approximately 248 – 458 kHz. This postulated noise is analyzed in the Supplementary Materials, where a PSD of the signal noise preceding the AE signal arrival demonstrates the same frequency content of 248 – 458 kHz (Fig. A4). No peaks are observed at 214 kHz, which indicates the 214 kHz peak is a deterministic signal amongst the high frequency noise, and this peak is the result of the low energy extensional AE mode. As previously stated, work is currently being done to reduce EMI and improve the sensor’s signal conditioning unit to further increase the sensor’s signal-to-noise ratio. With these improvements, the sensor is expected to capture a refined extensional mode signal. Nevertheless, the frequency content

of the extensional mode is not used within extensional mode AE source location techniques and only extensional mode time-of-flight between sensors is utilized due to its non-dispersive nature (10). Therefore, the slight discrepancy in extensional mode frequency content does not hinder the USM strain sensor’s potential for extensional mode-based AE source location. Flexural mode source location techniques do, however, rely on an accurate sensing of the frequency dispersion within a plate (24). As demonstrated by the nearly identical flexural mode frequency content between sensors, the USM strain sensor can also be potentially used in flexural mode AE source location. These findings illustrate the viability of the USM strain sensor’s ability to perform both extensional and flexural-based AE monitoring and source location, a crucial task within NDE and SHM currently performed by ultrasonic transducers. The sensor’s wide frequency bandwidth and low minimal detectable strain create the ability to be the first piezoresistive-based strain sensor capable of low energy AE sensing; additionally, these characteristics allow for the sensing of other important NDE measurements such as bending strain.

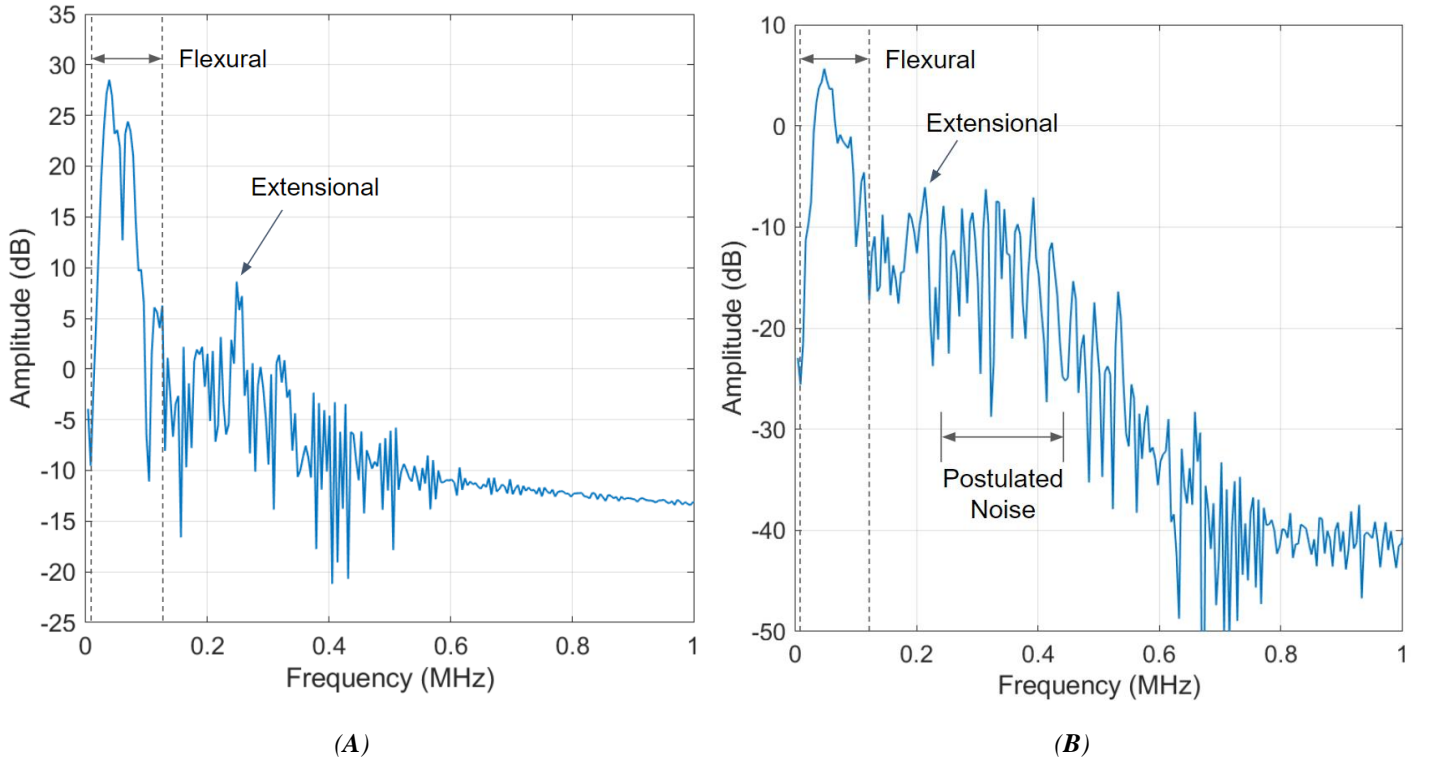


Figure 6. PSD of the filtered AE data from both sensor types. 0dB is 1 mW into 1 Ω . (A) Ultrasonic transducer PSD of recorded AE with labels denoting flexural vs. extensional mode frequency content. (B) USM strain sensor PSD of recorded AE. High frequency content beyond the extensional mode frequency range is attributed to EMI in the sensor signal and noise in the signal conditioning board. See fig. S5 in the Supplementary Materials for more information.

3.2 Sensor Response to Quasi-Static Bending

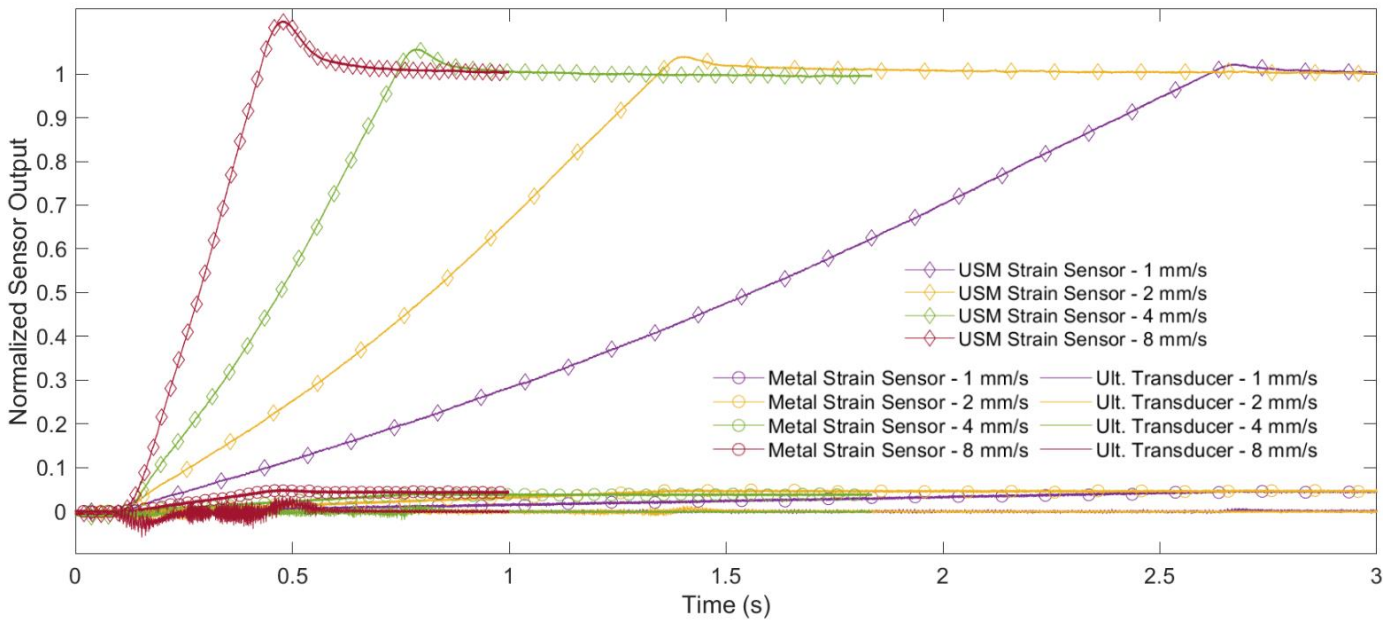
To have a true “dual application” sensor capable of both AE and bending strain measurements, it is necessary for the sensor to operate on a wide frequency bandwidth. The USM strain sensor’s ability to document a low energy, high frequency acoustic emission was demonstrated in the previous section; however, to evaluate the sensors’ responses to bending strain, both sensors were subjected to quasi-static loading at various loading rates. This in turn evaluates their potential for wide bandwidth, dual sensing applications.

The respective sensor responses to this loading are shown in Fig. 7A. The USM strain sensor outputs a steady linear response to the constant deformation of the applied load across the four loading rates. A clear differentiation in sensor response slope is noticed across the various loading rates due to the sensor’s sensitivity to bending. The commercial metal-based strain sensor documents a similar linear response to the loading but at a lesser magnitude. Additionally, the overshoot of the applied load is captured for each loading rate test. This overshoot, which is seen to be greater in the faster speed tests, is caused by an overshoot in the prescribed maximum load by the load frame machine; this is confirmed by the respective loading curves in Figure A7.

The ultrasonic transducer, however, provides only inertial responses. The limited response is due to a piezoelectric sensors’ ability to measure rapid strain changes but inability to retain surface charge (14, 15). By the nature of this testing, some inertial effects will be present at the beginning and ending of loading due to the acceleration and deceleration of the plate.

This implies that the loading test is not entirely quasi-static, particularly in the faster applied loads. The transducer captures the respective loading dynamics at the beginning and ending of loading but provides no significant response during steady-state, quasi-static bending. Fig. 7B demonstrates this comparison between the sensors’ responses by highlighting the steady-state loading region from 0.2 – 0.4 ms for the 8 mm/s bending test (shaded area in Fig. 7B) where bending is thought to be truly quasi-static. The calculated linear best-fit lines across this steady-state loading region shows the USM strain sensor’s strong response to quasi-static bending and the PZT ultrasonic transducer’s flat response.

To further analyze the respective sensors’ performance to bending strain, Figure 7C plots the respective sensor response slope during this region of quasi-static loading as a function of the applied loading rate. The resulting data points for the USM strain sensor create a linear best fit line with a slope of 286 mV/mm and a coefficient of determination (R^2) of 0.999. The strong linear correlation between the sensor output slope and applied loading rate demonstrates the USM strain sensor’s sensitivity to bending strain and in differentiating loading rates. The metal-based strain sensor is also capable of differentiating the loading rates with a R^2 of 0.999, but has over an order of magnitude lower sensitivity with a linear best fit slope of 7.99 mV/mm. The ultrasonic transducer, however, provides a near zero linear best fit slope with a R^2 of 0.311, denoting little to no correlation in sensor response and applied loading rate. This testing further demonstrates the transducer’s inability for quasi-static bending strain sensing (and therefore inability for dual application sensing of both high frequency and quasi-static loading cases) and further highlights the USM sensor’s potential for dual-application sensing.



(A)

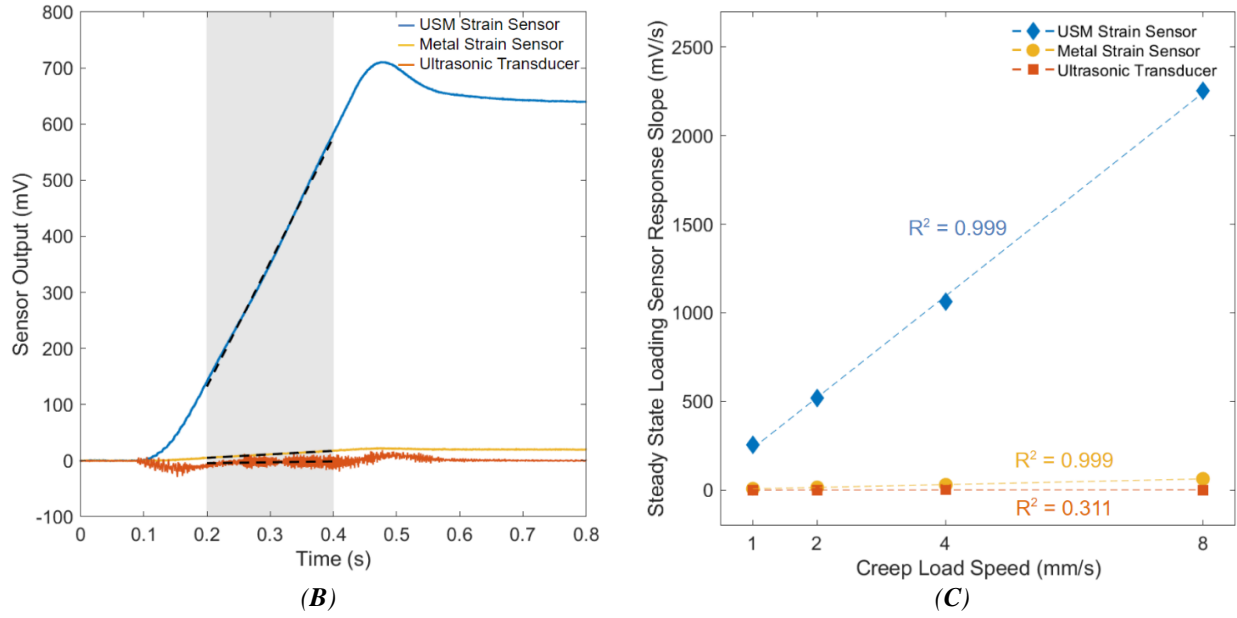


Figure 7. Bending strain performance of the USM strain sensor, metal-based strain sensor, and ultrasonic transducer when subject to quasi-static bending. (A) 500 Hz lowpass filtered responses of the sensors subject to plate bending across various constant loading rates up to a maximum load of 250 N. The y-axis is normalized to the USM strain sensor steady state output at a load of 250 N. Diamond and circular plot markers are utilized on response traces to differentiate between the USM and metal strain sensor responses, respectively; the ultrasonic transducer traces are solid lines with no markers. (B) Time history of the three sensor responses to the 8 mm/s applied load, highlighting the region of quasi-static loading from 0.2 – 0.4 ms where no acceleration of the loaded plate is present. A linear line of best fit for all respective sensor traces are plotted in this region. (C) The calculated slope of the sensor responses in the quasi-static loading region plotted as a function of the applied loading rate for the USM strain sensor (blue), metal strain sensor (yellow), and the ultrasonic transducer (orange), along with a best fit line and coefficient of determination calculated for all data sets.

4. CONCLUSIONS AND FUTURE WORK

The presented USM strain sensor aims to progress the field of NDE by improving the way stress and strain is recorded and analyzed when monitoring the health of a structure. Typically, a distributed network of permanently attached sensors, often including ultrasonic transducers and strain sensors, are employed to accomplish this (30). The presented USM strain sensor has been demonstrated to effectively combine the functionalities of both strain sensors and ultrasonic transducers by providing a wide frequency bandwidth response with a low minimum detectable strain. This includes an improved response to bending strain in the form of quasi-static bending typically characteristic of a piezoresistive strain sensor, and a comparable response in high frequency AE sensing typically monitored by ultrasonic transducers. This demonstration has shown the USM strain sensor to be the first known piezoresistive strain sensor capable of sensing an accurate low energy AE signal, including its low energy, high frequency extensional mode. The dual monitoring of quasi-static loading and high frequency acoustic emission enables the sensor for use as a permanent fixture to a structure to simultaneously provide *in situ* bending strain measurements and monitor AE events such as fatigue cracking, high velocity impacts, and delamination, and potentially source locate such events, all to

provide real-time evaluation towards the health of the structure. The combination of traditional strain sensor and ultrasonic transducer sensing capabilities within one singular miniaturized sensor can provide significant and novel improvements to the fields of NDE and SHM by not only reducing cost and instrumentation complexities, but by further advancing the field of NDE by applying modern MEMS technology.

The natural progression of the future of this work is to perform AE source location of PLBs as well as source location of impact events. These areas are currently being explored and preliminary results of both source location techniques are shown in Appendix B, which are shown to be very promising. Another area of interest is fatigue monitoring. Gorman (1991) has previously demonstrated the ultrasonic transducer's capability in differentiating fatigue cracking events from noise in a test specimen undergoing realistic flight fatigue loading (7). If the USM strain sensor were to be shown to be capable of making these same measurements, it would further strengthen its claim in being a novel NDE sensor capable of a wide variety of *in situ* measurements that assess the health of a given structure, all the while condensing the need for multiple sensor types, simplifying and improving NDE performance.

ACKNOWLEDGEMENTS

This material is based upon work in part supported by NASA under contract 80NSSC22CA085. We acknowledge Dr. William C. Wilson for his many insights and useful discussions of this work.

REFERENCES

- [1] J. N. Schoess, J. D. Zook, Conformal acoustic waveguide sensor development. *Smart Structures and Materials 1993: Smart Sensing, Processing, and Instrumentation*. **1918**, 90-96 (1993).
- [2] D. Chakraborty, M. E. McGovern, NDE 4.0: Smart NDE. *2019 IEEE International Conference on Prognostics and Health Management (ICPHM)*. 10.1109/ICPHM.2019.8819429 (2019).
- [3] T. Kundu, S. Das, K. V. Jata, Point of impact prediction in isotropic and anisotropic plates from the acoustic emission data. *The Journal of the Acoustical Society of America*. **122**, 2057–2066 (2007).
- [4] R. Gupta *et al.*, A Review of Sensing Technologies for Non-Destructive Evaluation of Structural Composite Materials. *J. Compos. Sci.* **5**, 319 (2021).
- [5] L. Huo, D. Chen, J.-N. Li, Structural health monitoring using piezoceramic transducers as strain gauges and acoustic emission sensors simultaneously. *Computers and Concrete*. **20**, 595-603 (2017).
- [6] M. G. R. Sause, Investigation of Pencil-Lead Breaks as Acoustic Emission Sources. *Journal of Acoustic Emission*. **29**, 184-196 (2011).
- [7] M. R. Gorman, Acoustic emission for the 1990s. *IEEE 1991 Ultrasonics Symposium*. **2**, 1039-1046 (1991).
- [8] A. K. Maji, D. Satpathi, T. Kratochvil, Acoustic emission source location using Lamb Wave modes. *Journal of Engineering Mechanics*. **123**, 154–161 (1997).
- [9] S. M. Ziola, M. R. Gorman, Source location in thin plates using cross-correlation. *The Journal of the Acoustical Society of America*. **90**, 2551–2556 (1991).
- [10] A. Tobias, Acoustic-emission source location in two dimensions by an array of three sensors. *Non-Destructive Testing*. **9**, 9–12 (1976).
- [11] K. Jeong, K.-J. Park, One sensor source localisation of acoustic emissions in thin plates using mode analysis. *Insight - Non-Destructive Testing and Condition Monitoring*. **61**, 264–270 (2019).
- [12] T. Kundu, S. Das, K. V. Jata, Point of impact prediction in isotropic and anisotropic plates from the acoustic emission data. *The Journal of the Acoustical Society of America*. **122**, 2057–2066 (2007).
- [13] K. M. Holford, D. C. Carter, Acoustic emission source location. *Key Engineering Materials*. **167-168**, 162–171 (1999).
- [14] K. Kim, J. Kim, X. Jiang, T. Kim, Static Force measurement using piezoelectric sensors. *Journal of Sensors*. **2021**, 1–8 (2021).
- [15] Y. G. Kim, J. H. Song, S. Hong, G. H. Ahn, Piezoelectric strain sensor with high sensitivity and high stretchability based on kirigami design cutting. *npj Flex Electron*. **6**, 52 (2022).
- [16] G. S. Kohil, T. Singh, H. Signh, Creep analysis in thick composite cylinder considering large strain. *Journal of the Brazilian Society of Mechanical Science and Engineering*. **68**, 42-68 (2020).
- [17] J. Wang *et al.*, Nonlinear creep model of salt rock used for displacement predication of salt cavern gas storage. *Journal of Energy Storage*. **48**, 103951 (2021).
- [18] D. Kuscer *et al.*, Acoustic Properties of Porous Lead Zirconate Titanate Backing for Ultrasonic Transducers. *IEEE Transactions on Ultrasonics, Ferroelectrics, and Frequency Control*. **67**, 1656–1666 (2020).
- [19] S. Sadeghpour, M. Kraft, R. Puers, Design and fabrication strategy for an efficient lead zirconate titanate based piezoelectric micromachined ultrasound transducer. *Journal of Micromechanics and Microengineering*. **29**, 125002 (2019).
- [20] M. Kobayashi, C. K. Jen, Piezoelectric thick bismuth titanate/lead zirconate titanate composite film transducers for smart NDE of metals. *Smart Materials and Structures*. **13**, 951 (2004).
- [21] A. R. Siddique, S. Mahmud, B. V. Heyst, A comprehensive review on vibration based micro power generators using electromagnetic and piezoelectric transducer mechanisms. *Energy Conversion and Management*. **106**, 728–747 (2015).
- [22] A. Carlson, A. M. Bowen, Y. Huang, R. G. Nuzzo, J. A. Rogers, Transfer printing techniques for materials assembly and micro/nanodevice fabrication. *Adv. Mater.* **24**, 5284–5318 (2012).

- [23] F. L. Marques dos Santos, B. Peeters, J. Lau, W. Desmet, L. C. Goes, The use of strain gauges in vibration-based damage detection. *Journal of Physics: Conference Series*. **628**, 1-8 (2015).
- [24] S. M. Ziola, “Source location in thin plates using crosscorrelation,” dissertation, Naval Postgraduate School, Monterey, CA (1991).
- [25] M. R. Gorman, Plate wave acoustic emission. *The Journal of the Acoustical Society of America*. **90**, 358–364 (1991).
- [26] N. N. Hsu, F. R. Breckenridge, Characterization and calibration of acoustic-emission sensors. *Materials Evaluation*. **39**, 60-68 (1981).
- [27] M. Popović, T. W. de Geus, and M. Wyart, Elastoplastic description of sudden failure in athermal amorphous materials during quasistatic loading. *Physical Review E*. **98**, (2018).
- [28] R. Beardmore, “Loaded Flat Plates,” *Mechanics Index*, 2020. [Online]. Available: https://roytech.org/Useful_Tables/Mechanics/Plates.html. [Accessed: 18-Apr-2023].
- [29] S. Timoshenko, S. Woinowsky-Krieger, “Chapter 5: Simply Supported Rectangular Plates,” in *Theory of plates and shells*, Ed. 2 (McGraw-Hill Education, 1959), pp. 105–173.
- [30] G. A. Matzkanin, Technology assessment of MEMS for NDE and condition-based maintenance. *Nondestructive Evaluation of Aging Aircraft, Airports, and Aerospace Hardware IV*. **3994**, 80-89 (2000).

ATTRIBUTIONS

Several individuals contributed to the presented work. Dr. Kang and Dr. Ruan from NanoSonic Inc. were responsible for the USM strain sensor design and fabrication and, along with Dr. Ng, for providing funding for the project. Albrey de Clerck and Noah Jones from NanoSonic Inc. contributed to all aspects of the project, especially in experimental design and setup and were of great help. Jason Smith and Marisa Gibbs assisted in experimental testing and data acquisition. Josh Deem from NanoSonic Inc. designed and assembled the signal conditioning box used in quasi-static bending testing. Shuo Mao helped provide extensive review of the original drafts of the journal article. Dr. Ng was involved in all aspects of this project, providing guidance every step of the way.

APPENDIX A: SUPPLEMENTARY MATERIALS

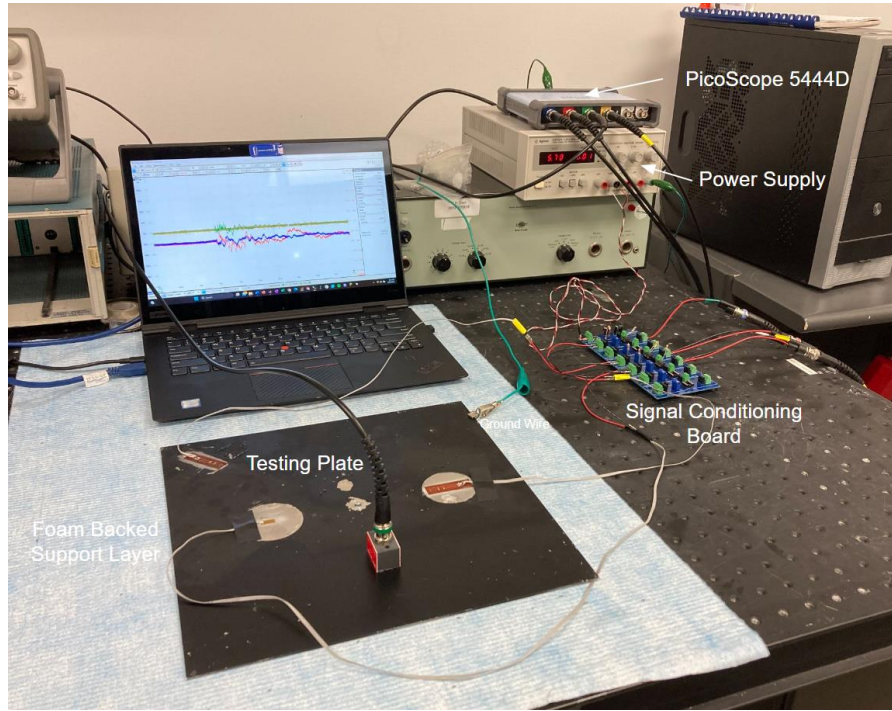


Figure A1. Experimental setup of the acoustic emission testing.

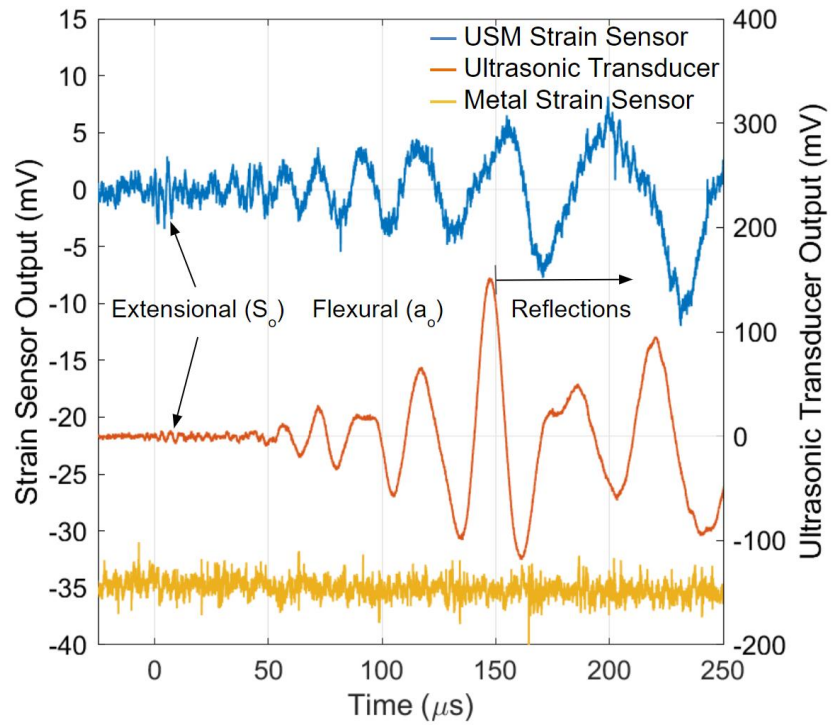


Figure A2. Unfiltered acoustic emission sensor signals. The USM strain sensor signal (blue trace) and the commercial metal-based strain sensor (yellow trace) are plotted on the same left y-axis scale; the ultrasonic transducer (orange trace), is plotted on the right y-axis scale. The unfiltered traces exhibit the same AE signal features as the filtered results but with additional noise.

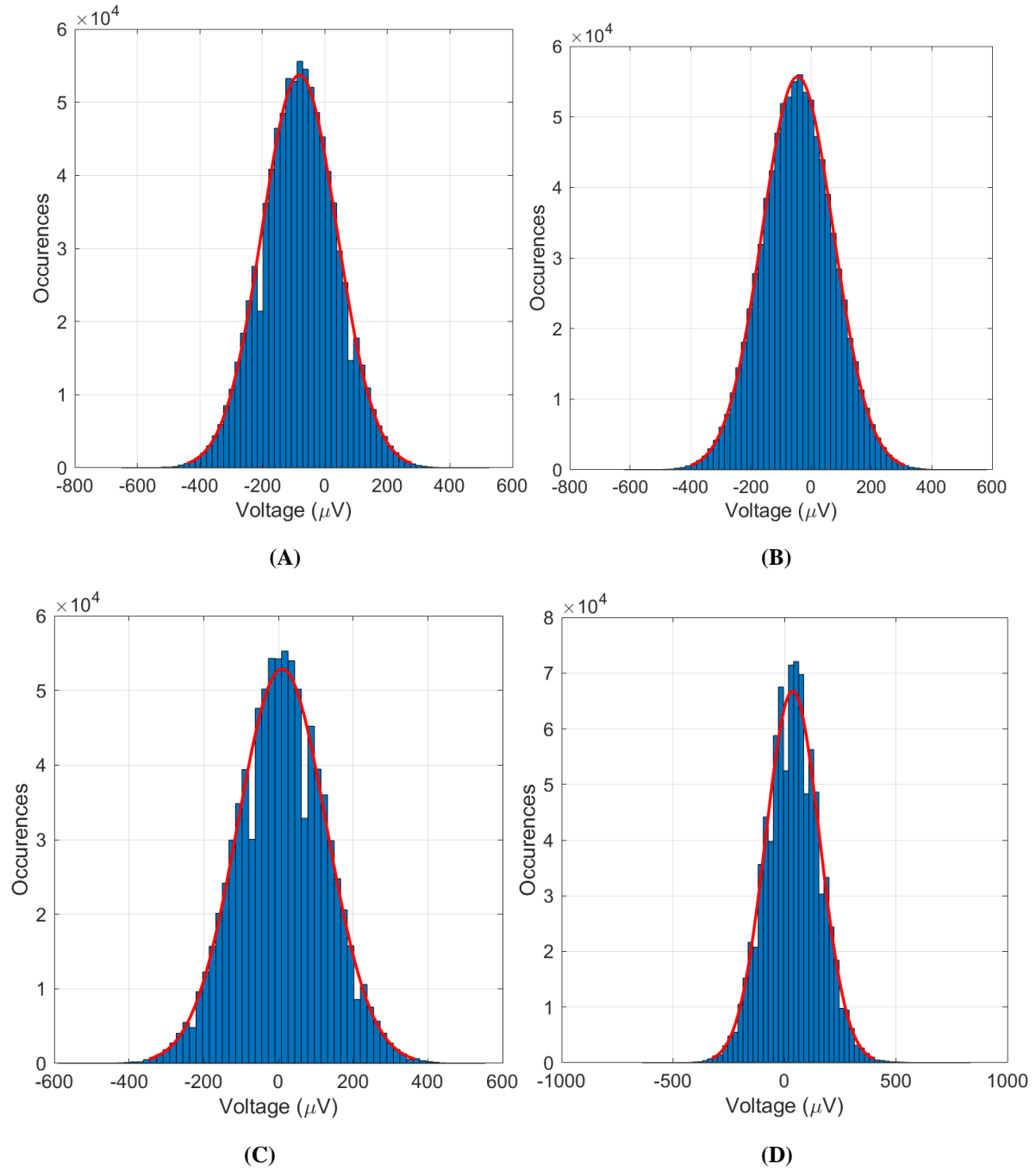


Figure A3. Analog to digital converter (ADC) noise in PicoScope 5444D used in experimental data acquisition. Shorted PicoScope channel data was collected at 17.86 MHz and a resolution of 12-bit to match the acoustic emission testing data acquisition setup. The resulting histograms of the shorted ADC data with an overlaid normal distribution and their bias error (mean) and RMS noise (standard deviation) are shown. The purpose of these calculations is to document noise that is inherent to the PicoScope's ADCs and not to sensor signal conditioning and electromagnetic interference (EMI). All units are in microvolts (μV). (A) Channel A: $\mu = -81.16$, $\sigma = 119.9$ (B) Channel B: $\mu = -44.31$, $\sigma = 118.2$ (C) Channel C: $\mu = 9.528$, $\sigma = 118.5$ (D) Channel D: $\mu = 36.70$, $\sigma = 121.0$.

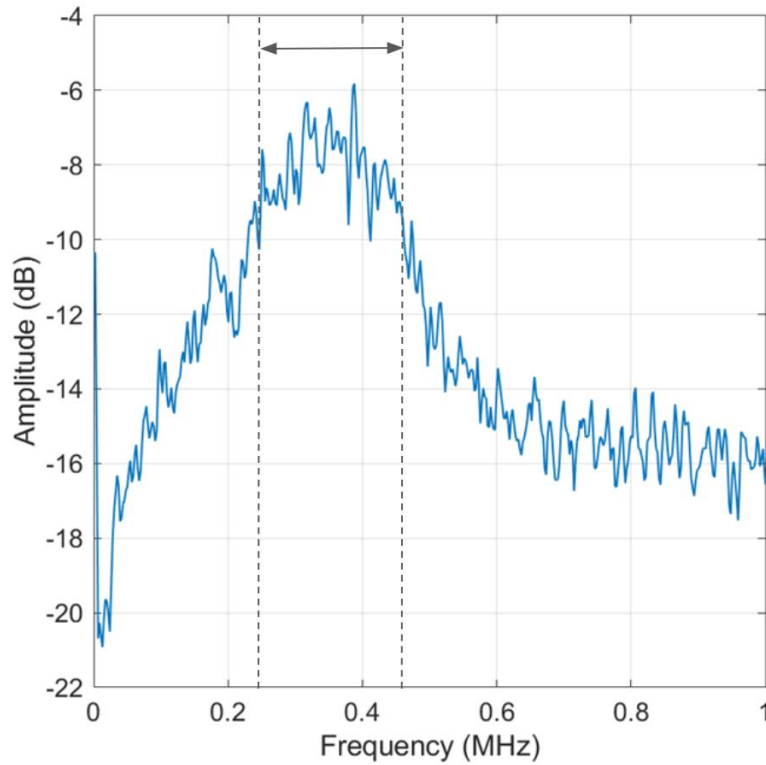
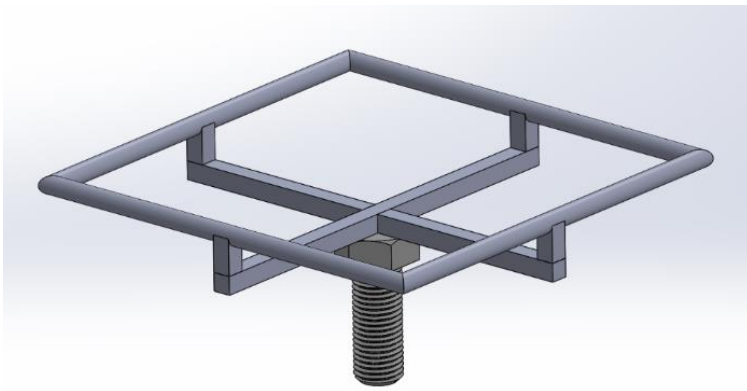
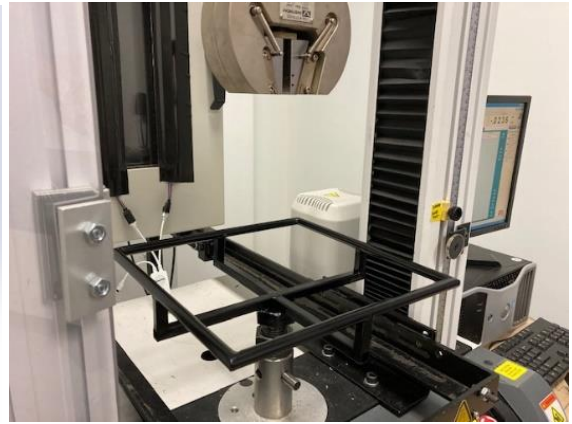


Figure A4. Power Spectral Density (PSD) of the unfiltered noise signal in the USM strain sensor. 0dB is 1 mW into 1 Ω . High frequency noise content is seen spanning from approximately 240 – 458 kHz, which is also observed in the PSD of the USM strain sensor AE signal (Fig. 3B). No peaks are observed at 214 kHz, which demonstrates the peak is a deterministic signal amongst the high frequency noise and is the result of the low energy extensional AE mode. The noise is expected to be a result of surrounding electromagnetic interference and the signal conditioning board.



(A)

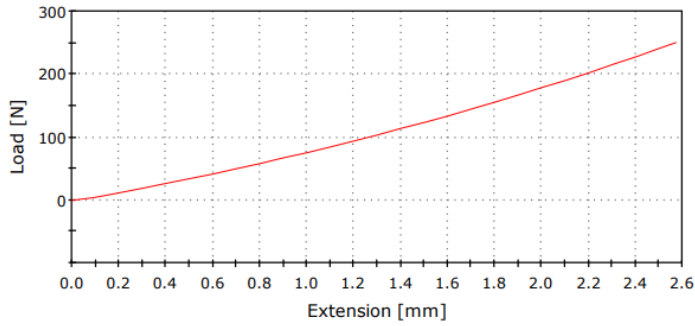


(B)

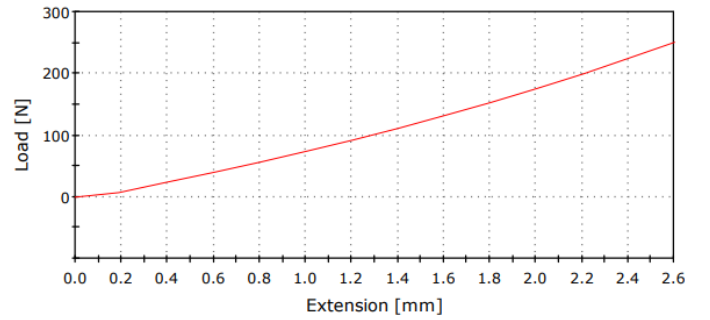
Figure A5. Custom-made static plate holder for quasi-static loading. (A) Final CAD design of the static plate holder created using SolidWorks. (B) The static plate holder within the Instron machine. The holder was manufactured from steel rods and welded onto a grade 8 bolt to fit in the Instron machine. The plate provides simply supported plate boundary conditions and is designed to fit the 12" by 12" by 0.087" aluminum 6061-T6 plate.



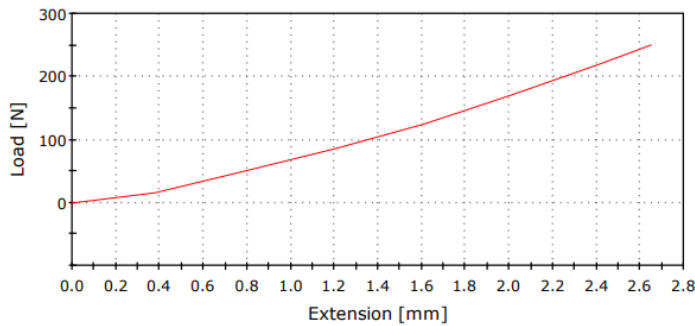
Figure A6. NanoSonic Inc. signal conditioning box used in quasi-static bending strain testing. The box uses a similar Wheatstone bridge configuration with potentiometers (seen as external knobs) to output strain sensor signals and houses its own internal power supply.



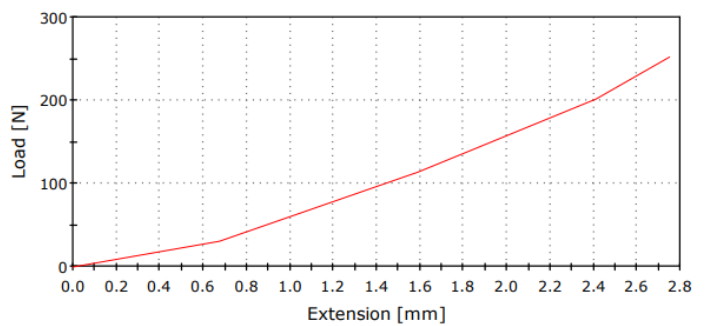
(A)



(B)



(C)



(D)

Figure A7. Instron loading curves for quasi-static loading experiments. The higher displacement rate tests finish past the end condition of 250 N, resulting in overshoot in the strain sensor signals. (A) 1 mm/s, loading begins at 0 N and ends at 250.1 N. (B) 2 mm/s, loading begins at 0 N and ends at 250.4 N. (C) 4 mm/s, loading begins at 0 N and ends at 250.6 N. (D) 8 mm/s, loading begins at 0 N and ends at 252.0 N

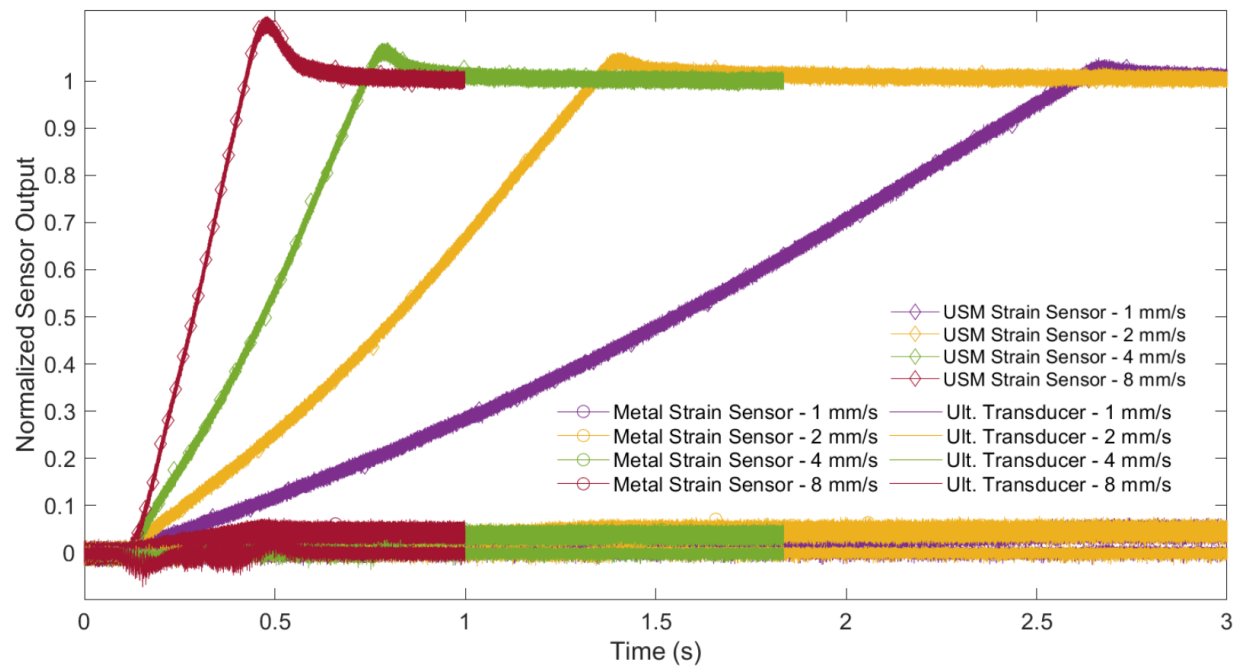


Figure A8. Unfiltered responses of the USM strain sensor, metal strain sensor, and ultrasonic transducer subject to quasi-static bending strain across various constant loading rates up to a maximum load of 250 N. A peak-to-peak noise level of approximately 15 mV is noted. The sensor responses exhibit the same signal features but with additional noise.

APPENDIX B: AE SOURCE LOCATION PRELIMINARY RESULTS

This section presents the promising preliminary work performed on the source location of acoustic emission events using the USM strain sensors. Due to limitations in sensor quantities (due to their manufacturing complexity and uses in other programs), only two USM strain sensors have been mounted so far to the testing plate. Tobias (1976) approached the problem of AE source location as three intersecting circles, each of which are centered at the receiving sensor and intersect at the AE source location (10). Since only two sensors are mounted on the plate (and of course, trilateration techniques require three sensors), the derivation of the AE source location equation can be reworked to show that for isotropic materials, the AE source location can be shown to lie on a hyperbola, with the two sensors as foci (9). The resulting equations for the x and y coordinates of the hyperbola of potential AE source locations are shown in Equations B1 and B2:

$$x(\theta) = \left[\frac{x_1^2 + y_1^2 - \delta_1^2}{2(x_1 \cos \theta + y_1 \sin \theta + \delta_1)} \right] \cos \theta \quad (B1)$$

$$y(\theta) = \left[\frac{x_1^2 + y_1^2 - \delta_1^2}{2(x_1 \cos \theta + y_1 \sin \theta + \delta_1)} \right] \sin \theta \quad (B2)$$

where x_1 and y_1 are the coordinates of sensor 2 relative to sensor 1, $\delta_1 = \Delta t * V$ where Δt is the time-of-flight difference of strain extensional mode arrival between sensors and V is the velocity of the extensional mode in aluminum. The resulting x and y coordinates are calculated for all values spanning zero to 2π radians. The preliminary results of AE source location of a PLB using this technique with the USM strain sensors is shown in Figure B1. The hyperbola of potential AE sources is off by less than an eighth of an inch; these results are comparable with calculations performed using ultrasonic transducers as a baseline test.

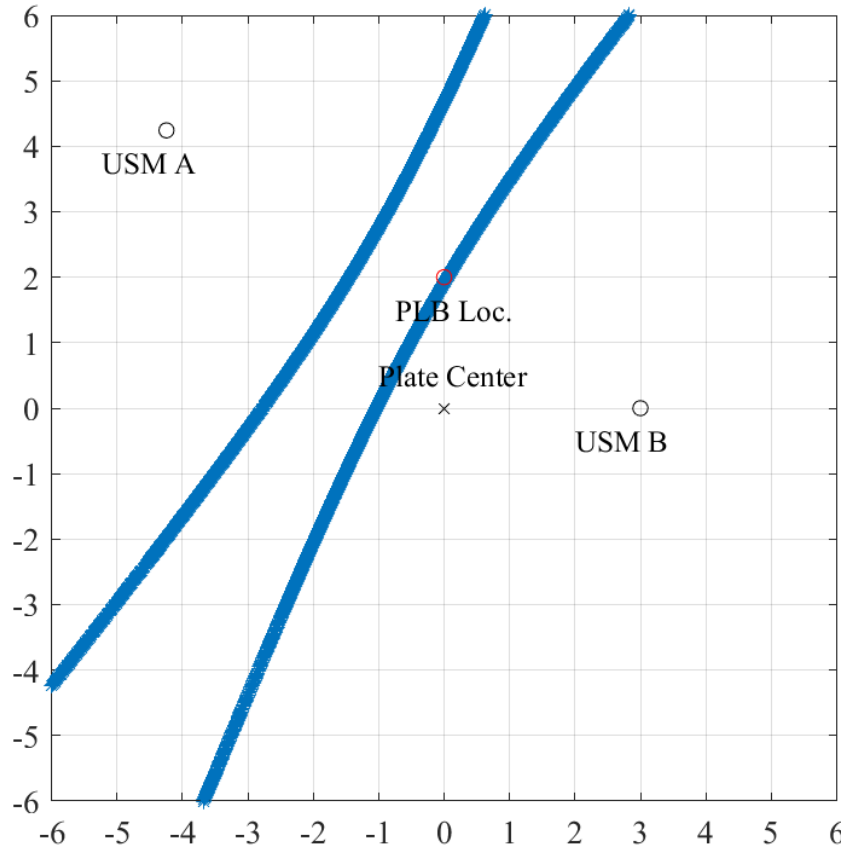


Figure B1. The “bilateration” of an AE source (PLB) on a 12 x 12 x 0.087-inch aluminum 6061-T6 plate using an extensional mode time-of-flight source location technique. The potential AE source locations are reduced to two hyperbolae. The resulting error is less than an eighth of an inch.

This technique, however, operates on the time-of-flight difference between sensors of the arrival of the extensional AE mode due to its non-dispersive nature. The extensional mode is typically much lower in amplitude than the subsequent flexural mode and is often damped out or is not seen in noisy systems. Gorman and Ziola (1991) published a method of AE source location in isotropic thin plates using cross-correlation, which can be used to perform AE source location on the much larger flexural mode (9). This technique involves cross-correlating the flexural mode AE signal with a cosine function modulated by a gaussian pulse. The modulated cosine function follows Equation B3 below:

$$x(t) = e^{-[(t-t_1)^2/\sigma^2]} \cos[\omega_1 t] \quad (B3)$$

where $\omega_1 = 6.283 \times 10^5$ rad/s ($f_1 = 100$ kHz), $t_1 = 100$ μ s, and $\sigma = 40$ μ s. These values were chosen to best match the initial flexural mode that arrives at the sensor before reflections interfere with the signal. The sensor signal and Equation B3 are cross-correlated, and the subsequent output function essentially isolates the time at which the chosen frequency (in this case 100 kHz) is present. The time-of-flight differences between sensors can then be used in Equations B1 and B2. This process was performed for a high velocity impact of a 2.16-gram ball bearing on the plate's surface, and the resulting "hyperbolic bilateration" is shown in Figure B2. The resulting preliminary results are off by about a quarter inch, which is very promising for the potential success of the source location of an AE event with the addition of a third USM strain sensor.

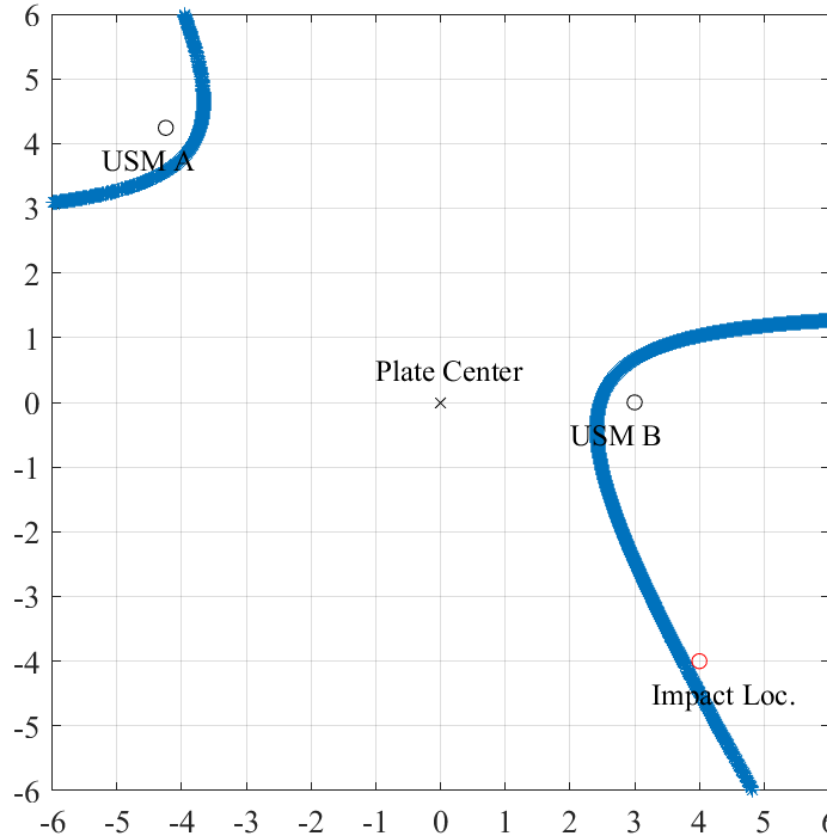


Figure B2. The “bilateration” of a high velocity impact (2.16-gram ball bearing) on a 12 x 12 x 0.087-inch aluminum 6061-T6 plate using a flexural mode cross-correlation-based AE source location technique. The potential impact locations are reduced to two hyperbolae. The resulting error is about a quarter inch.

APPENDIX C: OTHER NDE APPLICATIONS OF THE USM STRAIN SENSOR

This appendix includes other applications of the USM strain sensor to the field of NDE. Two applications are explored: USM strain sensor frequency detection on a vibrating plate and quantifying the energy of plate impacts. This work, in tandem with the completion of the work included in Appendix B, plans to be submitted to a journal at a later date.

C1. MATERIALS AND METHODS

C1.1 Vibrating Plate Testing

Chladni Plates – named after the German scientist and musician Ernst Chladni who first popularized the method by exciting a center fixed plate with a violin bow – produce intricate and beautiful patterns in plates (*C1*). Over two centuries after his initial discovery, these plates can now be seen in high school and university physics classrooms to demonstrate the intricate patterns present within plate mode shapes. Chladni's famous demonstration included exciting a center fixed support metal plate with a violin bow; the vibration of the plate, when oscillating in a particular mode of vibration, causes nodes and antinodes to form complex symmetrical patterns over the plate surface (*C1*). When sand (or any collection of fine grain particles for that matter) are placed on the plate surface these particles are displaced by antinodes and gather at the plate nodes, resulting in an observable intricate mode shape.

The experiment herein aims to utilize the USM strain sensor's sensitivity to low strain and broad frequency bandwidth to capture the modal frequency of the plate. The sensing and subsequent data processing of frequency content is common within NDE to analyze the health of a structure. Michael Gorman (1991) demonstrates this through the fatigue testing of a coupon-shaped aircraft specimen (*C2*). His testing demonstrates a noticeable difference in spectra between noise events and the propagation of a fatigue crack; this experiment demonstrates the importance of an accurate capturing of a vibrating structure's frequency content in NDE.

A more modern experimental setup is utilized to replicate some of Chladni's work and to demonstrate the USM strain sensor's response to a vibrating structure. In this experiment, a square 12" by 0.087" thick aluminum 6061-T6 plate is center mounted to a modal shaker capable of vibrating at frequencies spanning 5 – 7.5 kHz. A signal generator is used to supply sinusoidal signals across this frequency range to the modal shaker. A power amplifier is used to amplify the signal. The first series of experiments is performed with the plate to identify its modal frequencies and patterns. Subsequently, two USM strain sensors and a commercial metal-based strain sensor were affixed to the plate for sensor frequency response analysis.

Additionally, a model of the vibrating plate was created using COMSOL Multiphysics to provide a comparison to the plate mode shapes identified in testing. The model setup

consists of a 6" by 6" by 0.087" thick plate that utilizes quarter symmetry along two of its edges with the remaining two edges given a free boundary condition. The center of the plate is given a prescribed displacement boundary condition of 0.002", which closely matches the amplitude of the modal shaker. The model utilizes triangular shell elements, which assumes no thickness, since the thickness of the plate is small when compared to its length and width. A schematic of the model setup can be seen in Figure C2. A material of aluminum 6061-T6 was used to closely match the material of the tested aluminum plate. An eigenvalue study was performed to determine the model plate modal frequencies and patterns.

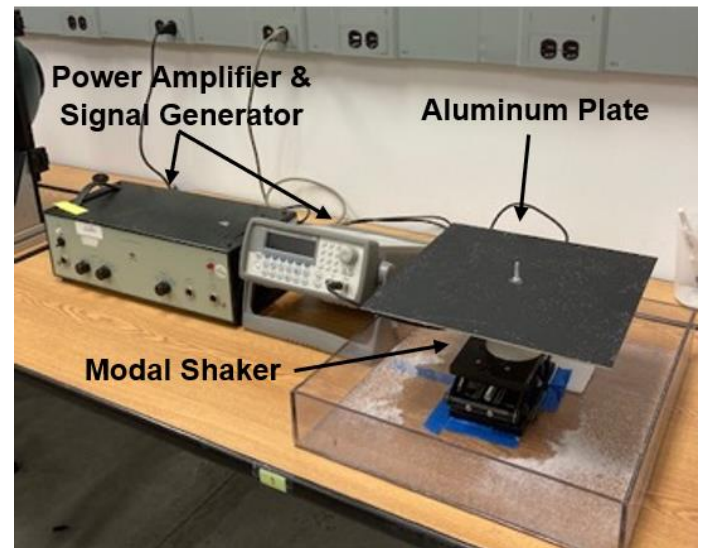


Figure C1. Experimental setup for vibrating plate testing. A Bruel & Kjaer Type 2713 power amplifier is attached to a signal generator, which all works to drive a Bruel & Kjaer V203 permanent magnet shaker with attached center-fixed 12" square aluminum plate.

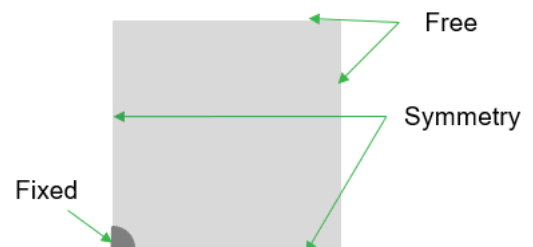


Figure C2. Schematic of the vibrating plate COMSOL Multiphysics model boundary conditions. Triangular shell elements were used with the material properties of aluminum 6061-T6.

C1.2 Low Energy Impact Studies

The goal of this test is to not only demonstrate the USM strain sensor's capability in detecting low energy impacts, but to establish the lower limit of the detectable energy and

establish a linear trendline between the voltage RMS and the potential energy of the drop. Two similar experiments were devised to demonstrate the USM strain sensor's capabilities in low energy impact sensitivity and time resolution. Both tests utilized a similar setup seen in Figure 4. The setup consists of a "dropping jig" that can drop ball bearings of various masses at various discrete heights, repeatably. The dropping jig also features a phototransistor mounted directly below the ball bearing, which documents the time of the release of the ball. The sensor signals are acquired and amplified utilizing a PCB quarter-bridge and is recorded using a PicoScope 5444D and laptop. An aerial view of the low energy impact study plate is shown in Figure C3.

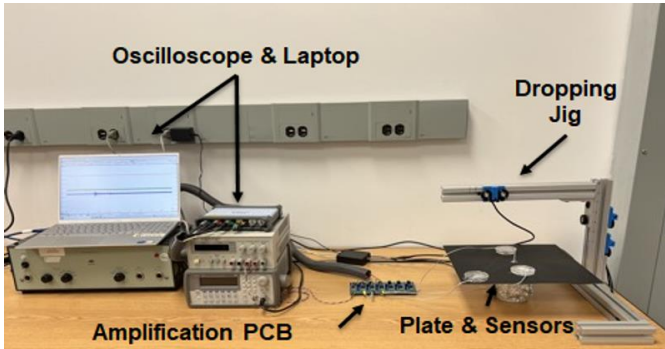


Figure C3. Drop testing experimental setup.

Two studies were performed; the first aimed to demonstrate the USM sensor's sensitivity to low energy impacts. Ball bearings of various mass were dropped from various heights directly between the two USM sensors at the location marked "C". The tested drop heights were from 1, 3, and 6 inches, and the ball bearing masses tested were 0.26, 0.9, and 2.13 grams. The second study aimed to demonstrate the time resolution of the USM sensors. A cascaded impact study was designed, which included dropping a ball bearing at seven different known locations between the two sensors to observe the latency between strain arrival at each sensor. The 2.13g ball was dropped from 6" for each test to provide the maximum excitation at that location.

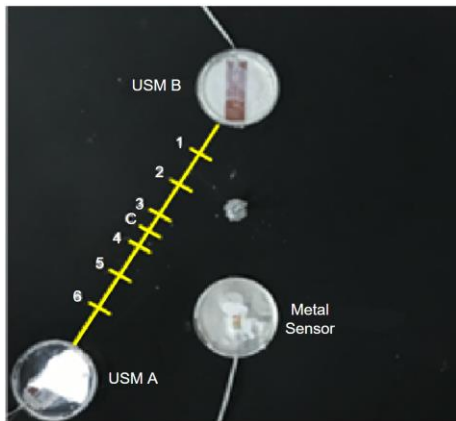


Figure C4. Impact study plate setup where the numbers and "c" mark the various drop locations between the two sensors.

C2. RESULTS AND DISCUSSION

C2.1 Vibrating Plate Testing

The eigenvalue study of the model provided very similar results to that of the vibration test, where six examples can be seen in Figure C5. The model closely matches the vibration test across the full range of tested frequencies where small frequency discrepancies are attributed to experimental uncertainties and element selection in the model. This validates the initial setup of the model; this model is intended to be used for strain calibration and comparisons at a later date.

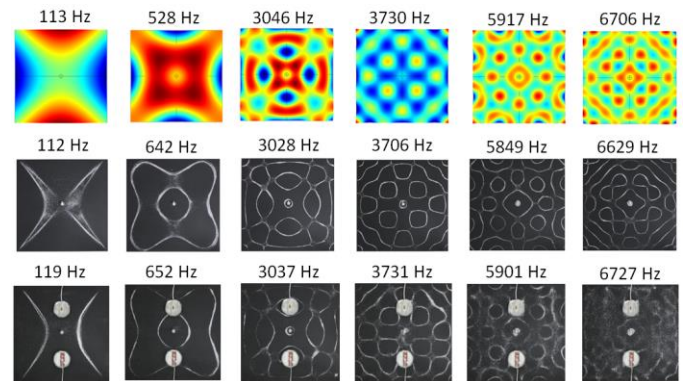


Figure C5. Six example mode shapes of a 0.087" thick aluminum plate across a frequency range of 5 Hz – 7.5 kHz compared to the model.

After the modal frequencies were retested with the strain sensors adhered to the plate, the Fast Fourier Transform (FFT) was computed for each case to analyze the sensors' responses in the frequency domain. Since USM B and the metal-based sensor are located symmetrically across the plate and are subject to the same strain, a direct comparison can be drawn between the two sensors' excitation magnitude. An FFT of five of the tested modal frequencies for USM B and the metal-based sensor are shown in Figure C6. The USM sensor responded with a higher sensitivity compared to the metal-based sensor across all tested frequencies. Notably, converting FFT peaks from dBu to voltage, the USM sensor recorded an excitation approximately 36 times greater at frequencies 669 Hz and 3037 Hz, and 28 times greater at 5901 Hz.

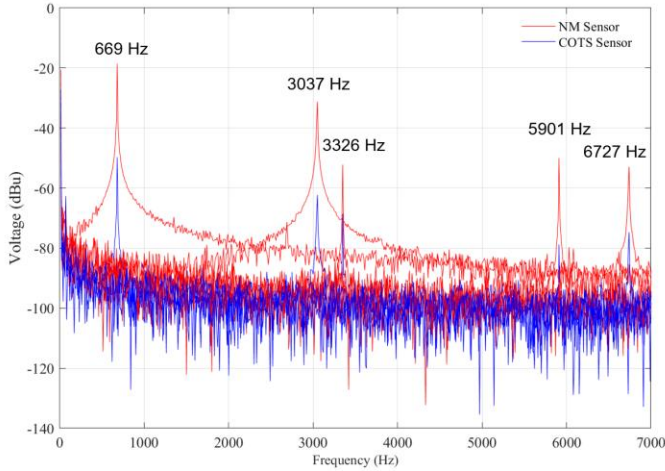


Figure C6. Comparing the frequency domain response of the USM and the metal-based commercial strain sensors across five plate modal frequencies.

C2.2 Low Energy Impact Studies

Example impact testing data is shown in the Figure C7, where the orange trace (right y-axis) is the signal from the phototransistor sensor used to trigger the data acquisition when the ball drops and the red, blue, and black traces are the signals from the strain sensors (left y-axis). Figure 13 shows a close-up of the data at the start of the strain sensor signals. From this data, it is seen that the metal-based sensor did not respond; the metal-based sensor did not respond to any drop tests.

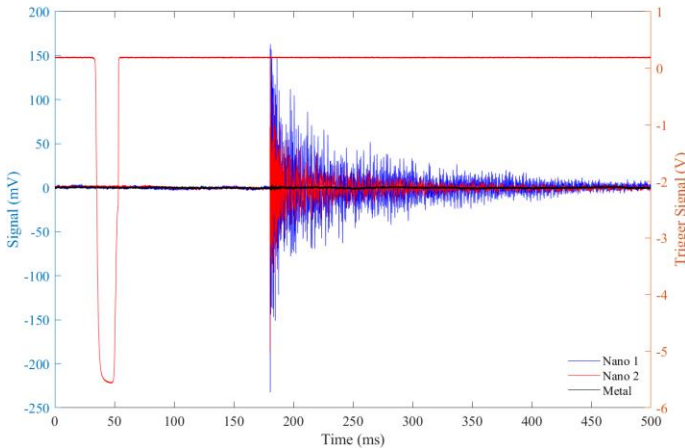


Figure C7. Recorded drop test data for the two USM and one metal-based strain sensor for location 1. The leftmost orange trace is of the phototransistor, which indicates when the ball was dropped.

In the first low energy impact study, which aims to evaluate the sensor sensitivity, the root mean square (RMS) of the recorded sensor voltage was calculated for each subsequent combination of mass and height of the ball, from which the initial potential energy of the drop was calculated. These two parameters are plotted against one another in Figure

C8 for the USM strain sensors. Both sensors respond linearly to an increase in initial ball potential energy. USM B indicates a lower sensitivity due to a smaller slope of the linear fit line, and this is attributed to the sensor's location in reference to the plate mounting point in the center. Shown in Figure C4, USM B is about half of the distance to the center mounting point as compared to USM A. Closer to the fixed center, it is expected that the plate's response is different as compared to the near free edge of the plate near USM A. Both USM sensors documented the low energy impacts whereas the commercial sensor was not able to detect any impact events.

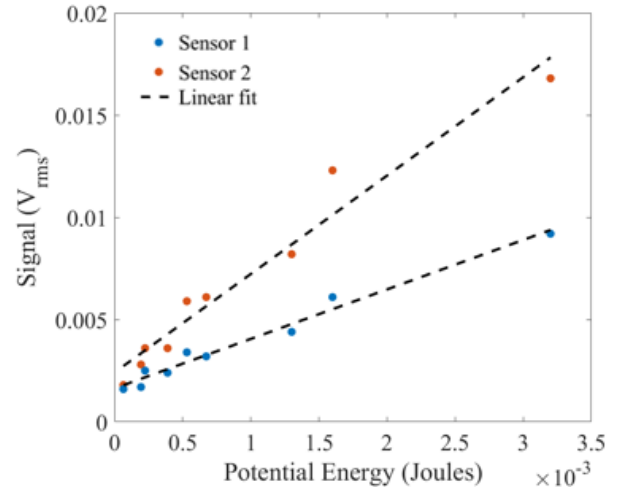


Figure C8. USM strain sensor recorded voltage RMS for various ball bearing drop heights and weights plotted as a function of the initial drop potential energy.

In the second low energy impact study which aims to evaluate the sensor's time resolution, the latency between strain arrival at each sensor is observed for various drop locations. An example of this latency is seen in Figure C9, where the latency between sensor strain arrival is taken as the time difference between respective initial sensor signal excitation. This data is for drop location 1 (see Figure C4); therefore, the signal arrives at USM B first and arrives at USM A at a time 49.9 μ s later. The metal-based strain sensor did not respond to any drops. This observed latency of strain arrival (taken as a time difference) between USM sensors is calculated for all seven drop locations on the plate. Figure C10 plots this time difference as a function of the drop location. The plot shows a strong linear relationship with a coefficient of determination (R-squared) of 0.9871, demonstrating the time resolution of the USM strain gauge for low energy impacts.

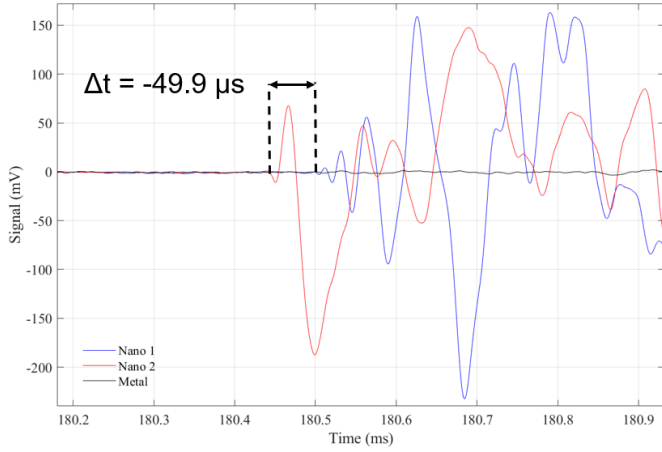


Figure C9. Observed latency of strain arrival between USM strain sensors at drop location 1.

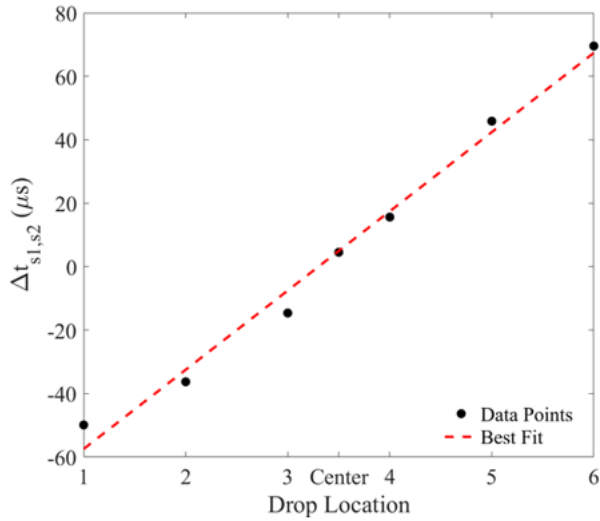


Figure C10. Observed latency of strain arrival between USM strain sensors as a function of seven drop locations.

These USM strain sensors can potentially be utilized for nondestructive evaluation purposes by utilizing its higher sensitivity and time resolution when compared to the commercial strain sensors. A group of ultra-bandwidth strain sensors may be used to record signals, then locate the precise location of an impact by measuring the time for the signals to reach different sensors.

References

- [C1] M. J. Gander and F. Kwok, Chladni figures and the Tacoma Bridge: Motivating PDE eigenvalue problems via vibrating plates. *SIAM Review*. **54**, 573–596 (2012).
- [C2] M. R. Gorman, Acoustic emission for the 1990s. *IEEE 1991 Ultrasonics Symposium*. **2**, 1039-1046 (1991).